Ion Induced Properties of Superconducting Rhenium Films

A. ul Haq
Institut für Angewandte Kernphysik

Kernforschungszentrum Karlsruhe

KERNFORSCHUNGSZENTRUM KARLSRUHE

Institut für Angewandte Kernphysik

KfK 3312

Ion induced properties of superconducting
Rhenium films.[*]

A. ul Haq

Kernforschungszentrum Karlsruhe GmbH, Karlsruhe

Abstract

Single-crystalline rhenium films have been prepared by electron beam evaporation on polished single-crystalline sapphire at various substrate temperatures T_s. Those with $T_s > 1100$ K show bulk behaviour at a superconducting transition temperature T_c (= 1.7 K) and resistivity at room temperature ρ_{RT} (= 18.0 $\mu\Omega$cm) .A residual resistivity ratio r between 15 and 22 was obtained for these films. Size effect measurements on films grown at 1300 K resulted in a value of 4.5×10^{-11} Ωcm^2 for the product $\rho(T) \times l_0(T)$, where l_0 is the mean free path of conduction electrons. Films grown at $T_s \leq 1000$ K had higher values of T_c and of the residual resistivity ρ_0. Annealing experiments indicated that these enhanced T_c- and ρ_0-values are due to defects, probably vacancies.

Intrinsic defects were produced in poly- and single-crystalline Re-films using 350 keV N- and 700 keV Ar-ions. The $\Delta\rho_0$ resistive and inductive T_c-enhancements as a function of deposited energy density Q are compared for the two ion species which were irradiated mainly at RT. The increase in $\Delta\rho_0$ up to 10^{25} eV/cm^3 is independent of the ion type. At low fluences the increase in ρ_0 is attributed mainly to vacancies and at high fluences to the formation of extended defects. Intrinsic defects caused an increase of 2.5 K in the inductive T_c-value. The increases in resistive T_c-values were independent of the ion species. The T_c-enhancement is probably caused by vacancies pinned to dislocations, extended defects alone do not seem to have any influence on T_c. Isochronal annealing of ρ_0 and inductive T_c supported these findings.

Impurity defect complexes produced by Ar- and N-implantations at a constant Q-value caused the same increase in T_c. Inductive T_c appears to saturate at 3.0 K. For N-defect complexes higher ρ_0-values are obtained as compared to Ar-defect complexes.

Two metastable rhenium nitride phases namely ReN$_{0.09}$ and ReN were observed after implantation of N-ions. High stress values were obtained in the Re-films during the formation of these phases. The structure of ReN$_{0.09}$ could not been identified. However, ReN was identified as a fcc(B1) structure whose lattice parameter was found to depend on the N-concentration. The highest T_c observed by 9 at% N was 4 K whereas for ReN it was 4.5 to 5.0 K. Implantation of N-ions above 42 at% at LNT[*] produced an X-ray amorphous phase with a T_c-value of 6 K. An amorphous Re-phase was also obtained by 20 at% P implanted at LNT with a T_c-value of 7 K.

[*]liquid nitrogen temperature

Ionen-induzierte Eigenschaften von supraleitenden Rheniumschichten

Zusammenfassung

Rhenium Schichten wurden durch Aufdampfen mit einer Elektronenstrahl-kanone auf polierte, einkristalline Saphir-Substrate unter verschiedenen Bedingungen hergestellt. Bei Substrattemperaturen, T_s > 1100 K waren die aufgedampften Schichten einkristallin und zeigten für viele Eigenschaften Werte des massiven Materials (T_c = 1.7 K, Widerstand bei Raumtemperatur = 18.0 $\mu\Omega$cm). Aus Sizeeffekt-Messungen an Schichten die bei 1300 K aufgedampft worden waren, wurde ein Wert von 4.5 x 10^{-11} Ωcm^2 für das Produkt $\rho(T) \cdot l_o(T)$ bestimmt, wobei l_o, die mittlere freie Weglänge für Leitungselektronen in Re ist.

Zur Erzeugung von Eigendefekten wurden poly- und einkristalline- Re-Schichten mit 350 keV N- und 700 keV Ar-Ionen bei RT durchstrahlt. Es wurde eine Erhöhung von $\Delta\rho_o$ sowie der resistiv- und induktiv-gemessenen T_c-Werte als Funktion der deponierten Energiedichte, Q beobachtet. Die Zunahme von bis zu Q-Werten von 10^{25} eV/cm^3 ist unabhängig von der Ionensorte und wird der Existenz von Punktdefekten zugeordnet. Die starke Erhöhung von $\Delta\rho_o$ für große Q-Werte wird der Existenz von Versetzungen zugeschrieben. Resistiv gemessene T_c-Werte hängen von den T_c-Werten der unbestrahlten Probe ab. Induktiv gemessene T_c-Werte haben einen maximalen Wert von 2.5 K für Eigendefekte.

Es wurde erwartet, daß neben dem Einfluß von Eigendefekten bei der Ionenimplantation zusätzliche Effekte auftreten. Zur Klärung dieser Frage wurden zunächst einige at% Ar- und N-Atome durch Implantation bei Raumtemperatur homogen verteilt in die Schichten eingebaut. Ein Vergleich zwischen den Ergebnissen von Durchschuß- und Implantations-Experimenten bei gleichen Q-Werten ergab einen maximalen T_c-Wert von 3 K nach Ar- und N-Implantation, möglicherweise hervorgerufen durch die Bildung von verunreinigungsstabilisierten Defekt-Komplexen. Allerdings zeigten die mit Stickstoff implantierten Schichten größere ρ_o-Werte als Ar-implantierte Schichten.

Mit wachsender N-Konzentration bilden sich zwei metastabile Phasen $ReN_{0.09}$ sowie ReN. Die Phasenbildung ist von dem Auftreten höherer Spannungen in den Re-Schichten begleitet. Die Struktur von $ReN_{0.09}$ konnte nicht identifiziert werden. ReN hat eine fcc(B1) Struktur und der Gitterparameter hängt von der N-Konzentration ab. Der höchste induktiv gemessene T_c-Wert beträgt 4 K bei 9 at% N. Der maximale T_c- sowie ρ_{RT}-Wert für ReN war 5 K bzw. 230 $\mu\Omega$cm. Nach der Implantation von 42 at% N bei LNT wurde die Re-Schicht röntgenamorph, d.h. alle Röntgen-Reflexe verschwanden. Dabei wurden maximale ρ_{RT}- sowie T_c-Werte von 320 $\mu\Omega$cm bzw. 6 K beobachtet. Eine amorphe Phase stabilisiert durch 20 at% P bei LNT hat einen T_c-Wert von 7 K.

C O N T E N T S :

Abstract

Zusammenfassung

1. Introduction

Pure and defect free single crystals of rhenium have a superconducting transition temperature, T_c, of 1.7 K and room temperature (RT) resistivity of 18.0 $\mu\Omega$cm /1,2/. Rhenium crystallizes in hexagonal close packed structure with lattice parameters, a = 2.760 Å and c = 4.458 Å, and belongs to the 7th group of the periodic table with 7 valence electrons/atom, (e/a). According to the empirical rule of Matthias, the T_c of transition metal alloys can be predicted using only the average number of e/a. The experimental curve for T_c as a function of e/a shows a maximum in T_c for a value of 6.5 /3/. Thus alloying of Re with other transition metals lying on the right (left) side of it in the periodic table, would lead to an increase (decrease) of T_c. Further in terms of Miedemas theory /4/, it is expected that impurities with an electronegativity smaller (larger) than that of Re would increase (decrease) T_c. Chu and co-workers /5/ observed, however, that T_c of Re increased with small additions of impurities from either side of the periodic table in contrast to other superconductors. This anomalous behaviour of Re has also been observed by other authors /6,7/.

It has been observed by Hauser and Buehler /8/ that T_c of Re-single crystals increases if annealed to higher temperatures and subsequently quenched. They also noted that plastic deformation does not affect T_c of a well annealed Re single crystal, however, it caused increase of T_c for an as-grown crystal. These effects were attributed to vacancies. Kopetskii et al. /9/ studied the plastically deformed Re-single crystals with the help of annealing and quenching experiments and concluded that vacancies and dislocations have a marked influence on the change in T_c. Thus not only alloying of impurities but also defects will affect T_c of Re. However, the possibility of the formation of impurity-defect-complexes cannot be excluded, as well and might be responsible for T_c-enhancements.

To explain this phenomenon the above mentioned workers /8,9/ have assumed the following: since the band structure of Re has singularities in the electron density of states near the Fermi level, $N(E_F)$, and the Fermi level is located at the front edge of the singularity /10,11,12/, enhanced scattering by impurities or defects would cause a smearing of the peak near $N(E_F)$. Thus an increase in $N(E_F)$ may be responsible for the observed T_c-enhancements.

Polvov et al. /13/ have shown that plastic deformation in Re-single crystals produced an increase in the specific heat but electron density of

states did not change within 5%. The increase in specific heat is explained by reduction of the Debye temperature and as a result, softening of the phonon spectrum is supposed to be responsible for the increase in T_c. However, the question remains open about the nature of defects which caused the increase in specific heat and T_c.

To test further the validity of the Miedemas theory, Meyer /7/ has implanted many elements with a wide range of electronegativity values in Re-thin films. He observed that the implantation of S-, B-, Cs-, N- and Zn-ions up to 40 at% increased the T_c in each case up to 4.5 - 5.0 K, whereas implantation of Zr-, Ti- and Y-ions enhanced T_c by 1 - 3 K/at% (up to 9 K). No explanation was presented for the observed T_c-enhancements. In these experiments implanted ions came to rest in the rhenium films. Therefore not only intrinsic defects are produced but due to the presence of impurities, impurity-defect-complexes or metastable phases may also be formed.

The aim of the present work was to separate the influence of the various above mentioned effects on resistivity, T_c and structure of the Re-thin films. Ion implantation and ion irradiation is thought to be the best tool to produce such effects separately and has, therefore, been utilized for this purpose. Use of chemically inert ions with sufficiently high energy would create only intrinsic defects if irradiated through the films. Therefore the study of ion irradiation requires that the film thickness should be much smaller than the mean projected range of the ions, R_p. Similarly for homogeneous ion implantation experiments, the energies of the ions are so selected that ions come to rest in the film and could produce impurity-defect-complexes or metastable phases. The metastable phases could be detected by X-ray diffraction.

The essential condition for performing such experiments is to prepare high quality Re-thin films with bulk properties e.g. RT-resistivity, T_c etc. It is further necessary that the thickness dependence of the resistivity and T_c should be known. This is required to avoid the increase in resistivity resulting from size effect. Thus the film thickness should be greater than the mean free path of conduction electrons, l_o.

In the following chapter (2), the sample preparation and experimental methods are described. The results of the present study are presented in chapter 3, which is divided in to three sections. In the first section the influence of preparation parameters such as substrate material, substrate temperature etc. on T_c, resistivity and the structure of the thin films is presented and the thickness dependence of resistivity is used to determine l_o. In the second section the influence of intrinsic defects produced by Ar-

and N-ion irradiation on the resistivity, T_c and structure is described. The nature of the defect structure is studied by isochronal annealing experiments. In the last section of this chapter homogeneous ion implantation experiments are described. The Ar-ions are used to study the influence of mechanical effects such as development of high stresses in film, whereas N-ions are used to produce impurity stabilized defects and metastable phases as a function of ion concentrations. The P-ions are used to create an amorphous phase of the Re. The discussion and conclusions of this study are presented in the last chapter.

2. Experimental Methods

2.1 Film Preparation:

An electron beam gun with a maximum input power of 6 kW was used to deposit the films from high purity double-zone refined rhenium in an UHV chamber. The pressure in the chamber was typically 1×10^{-8} Torr before the electron beam was focused on the rhenium cylinders and rose to 1×10^{-5} Torr after the beam was turned up to the intensity used for evaporation. Then the pressure dropped slowly and evaporation was continued for about two minutes before the shutter was opened for the film deposition. At this stage the pressure was typically 1×10^{-7} Torr.

The evaporation rate could be varied by changing the input power of the electron gun. This was varied between 1 and 20 Å/sec. Different substrate materials such as carbon, quartz and sapphire were used but films were mainly grown on polished sapphire substrates (also called polished substrates). Films were also evaporated onto rough sapphire substrates (also called rough substrates). To obtain rough substrates, the polished substrates were gently lapped on wet boroncarbide (grain size $\sim$ 300 mesh) for a few minutes until the surface was no longer shining. Then the substrates were rinsed successively in water, methanol and acetone to remove the dust particles.

The substrates (of dimensions 25 mm x 5 mm x 1 mm) were mounted on a Mo-sample holder which could be heated by electron bombardment. The substrate temperature, T_s, was varied between room temperature (RT) and 1330 K and was measured by a pyrometer.

2.2 Ion Implantation of Thin Films:

In this work two different types of ion beam irradiation were performed. In ion implantation experiments, impurity atoms were nearly homogeneously introduced within the film thickness. In ion irradiation experiments, ions had energies high enough to penetrate through the Re-films and came to rest in the substrate, thereby producing only defects due to the interaction of the ions and the Re-atoms. In such experiments the stopping of the irradiated ions, their range straggling and distribution of defects which depend on the penetration depth at which the concentration of implanted ions reaches its maximum value, are of considerable importance. These have been discussed in detail in the literature /14-16/.

For both the above mentioned experiments a 350 keV heavy ion accelerator installed in the "Institut für Angewandte Kernphysik I, Kernforschungszentrum Karlsruhe" was used. The construction and the principles of this accelerator have already been described in detail by Langguth [17] and Ziemann [18]. During ion implantation the vacuum in the beam line was 10^{-6} Torr while in the implantation chamber it was 10^{-7} Torr. An aperture system was used before the sample so as to suppress the secondary electrons which in turn helped to determine the fluence from the amount of (ion-) current passing through the sample.

2.2.1 Ion Irradiations:

For these experiments the rhenium films were irradiated with 350 keV N-ions and 700 keV Ar-ions at RT as a function of ion fluence in the range of 10^{12} to 2×10^{17} ions/cm^2. The temperature dependence of the irradiations was also studied. For this purpose, Ar-ion irradiation were performed at liquid nitrogen temperature (LNT). The ion current during RT irradiation was between 3 and 6 A/cm^2 and for LNT, it was 1 A/cm^2.

The mean projected range, R_p and the energy density profiles of the bombarding ions were calculated employing a computer programm of Biersack and Haggmark [19]. The 350 keV N- and 700 keV doubly charged Ar-ions in Re have a R_p-value of about 1903 Å and 1861 Å, respectively. For N-ion irradiations, Re-films of a thickness from 600 to 1400 Å were used whereas for Ar-ion irradiations, the thicknesses were 740 to 1200 Å. The deposited energy density from nuclear collisions in addition to other processes for N-ions increased from 8 to 20 eV/Å within the film thicknesses used. For Ar-ions, it was 69 eV/Å at the surface and increased to 105 eV/Å at a depth of 1200 Å.

In order to estimate the cross-section for primary collisions, σ_d, the mean energy transferred in such a collision, $\bar{T}$, the mean free path of the bombarding ions, l_{pk}, and the concentration of the displaced atoms, C_d, due to 2×10^{17} ions/cm^2, a Nielsen potential has been used [20]. The calculated values for 350 keV N-ions and 700 keV Ar-ions are summarized in Table 1. The average threshold energy used in these calculations for defect production in polycrystalline Re thin films is 40 eV [21]. Since l_{pk} for Ar-ions is 24 Å as compared to 63 Å for N-ions, the density of defects produced along the track of Ar-ions is higher in comparison to N-ions.

Table 1

Comparison of damage production parameters for
350 keV N-, and 700 keV Ar-ions.

	350 keV N$^+$	700 keV Ar$^+$
R_D/Å	2200	1772
(DE/dx) Nuclear eV/Å	8-20	69-105
Average Number of vacancies/ion/Å	2.3	15.0
C_d/cm^3	9.5 x 10^{24}	5.3 x 10^{25}
σ_D/cm^2	2.38 x 10^{-17}	6.24 x 10^{-17}
$\bar{T}$/eV	1509	3191
l_{pk}/Å	63	24

2.2.2 Homogeneous Ion Implantations:

The homogeneous ion implantation (also called ion implantation)
experiments were performed with Ar-, N- and P-ions. Ar-ions were implanted
only at RT while P-ion implantations were carried out mainly at LNT. N-ions
were implanted at 475 K, RT and LNT. Three different energies were used to
obtain a homogeneous implantation profile which was calculated with a compu-
ter programm /22/ using R_p and ΔR_p values based on LSS theory /23/. Table 2
gives some of the calculated energies and fluences used to obtain homogene-
ous profiles of Ar-, N- and P-ions and such a calculated profile for N-ions
in Re (700 Å) is shown in Fig. 1. Except for the surface region, a reasonable
homogeneous distribution is seen.

The homogeneity of the implantation as a function of the depth was
tested by Rutherford backscattering (RBS) of 2 MeV He-particles as de-

Table 2

Calculated energies and fluences necessary to get a homogeneous implantation profile for different ion-target (rhenium) combinations and film thickness. The value of R_p and ΔR_p used for these calculations are also given in the table. The given fluence values produce a concentration of 1% At implanted ions.

Ion	Film thickness/Å	Energies (keV)	R_p/Å	ΔR_p/Å	Fluences (ions/cm^2)
N$^+$	560	20	137	117	9.57E14
		60	376	170	7.20E14
		130	822	518	8.55E15
N$^+$	700	20	137	117	1.09E15
		60	376	170	6.75E14
		110	693	393	6.27E15
N$^+$	900	20	137	117	9.58E14
		60	376	170	8.05E14
		140	886	556	9.22E15
N$^+$	1190	30	198	140	1.36E15
		100	629	220	8.56E14
		170	1080	646	1.04E16
N$^+$	2100	50	316	167	1.20E15
		110	693	393	3.63E15
		300	1916	920	1.52E16
P$^+$	560	30	108	47	1.80E14
		70	225	169	1.41E15
		240	720	419	6.93E15
Ar$^+$	1300	60	170	135	1.09E15
		170	434	266	2.66E15
		460	1162	564	9.28E15
Ar$^+$	1520	80	219	152	1.27E15
		220	554	324	2.90E15
		550	1390	641	1.05E16
Ar$^+$	2000	50	146	232	2.66E15
		280	705	390	3.87E15
		700	1772	758	1.24E16

ARBITRARY
UNITS

110 KeV

N^+——Re (700 Å)
1%

30 keV: $1.09 \cdot 10^{15}$ N^+/cm^2
60 keV: $6.75 \cdot 10^{14}$ N^+/cm^2
110 keV: $6.27 \cdot 10^{15}$ N^+/cm^2

30 KeV

60 KeV

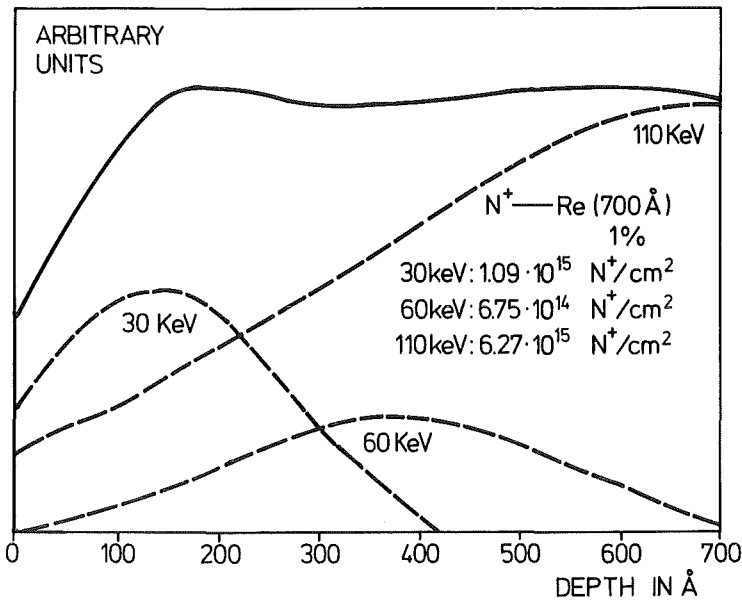0   100   200   300   400   500   600   700

DEPTH IN Å

Fig. 1
Calculated implantation pro-
file for N in Re (700 Å).
The implantation energies and
their fluences are for 1% At.

scribed in the next section. Such an RBS spectrum of a Re-film before and
after the implantation of 45% At N is shown in Fig. 2. In the RBS spectrum
of an implanted sample, a decrease in the peak height accompanied by an
increase in peak width is registered as compared to the unimplanted sample.
This is due to the increased energy loss of He-particles through the im-
planted N-atoms. The smooth plateau indicates the homegeneous distribution
of the N-ions in the Re film. The total peak area is indpendent of the
energy loss and is proportional to the number of Re-atoms. In the calculated
profile there was an inhomogeneity at the surface region of about 150 Å
which could not be observed in the RBS spectrum. This may be a result of the re-
solution limit of the RBS method or of sputtering effects.

54

42

Re

Re + 45% At N

COUNTS × 1000

30

2100 Å

18

6

0
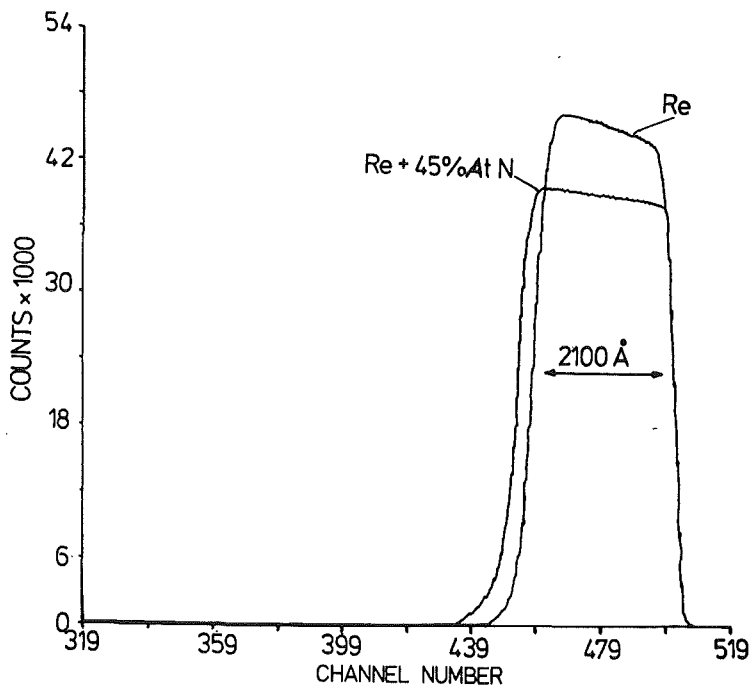319   359   399   439   479   519

CHANNEL NUMBER

Fig. 2
RBS spectrum of an Re film,
before and after implanta-
tion of 45% At. N. The smooth-
ness of the plateau for im-
planted film indicates that
implanted ions are homogene-
ously distributed.

2.3 Rutherford Backscattering (RBS)

RBS was used to determine the film thickness, homogeneity and concentration of impurities. For these measurements a monoenergetic beam of 2 MeV He-particles obtained from a Van de Graaff accelerator was used perpendicularly to the film under investigation. The number of the backscattered particles as a function of energy were registered with a silicon surface barrier detector located at 165°, equipped with a preamplifier, main amplifier, ADC and a multichannel analyser. The He-particles will be scattered with higher energy from heavy elements as compared to the light ones. Thus using a calibration sample under the same experimental conditions, it is possible to identify different elements present in the film. The peak height at a particular energy is a measure of the quantity of that element and the peak width is a measure of the film thickness, t, given by /24/

$$t = \frac{\Delta E}{[\varepsilon]} \cdot [N]^{Re}$$

where

ΔE: width at half maximum of the Re-peak on the energy scale,

$[N]$: atomic concentration of Re,

$[\varepsilon]$: stopping cross-section factor for 2 MeV He-particles in Re.

The factor $[\varepsilon]$ takes into account the energy loss of the incident He-particles during backscattering. This must be calculated from the stopping cross-section and kinematic factor of the target (Re) atoms /24/. These values are tabulated in Ref. /25/. Thus

$$\frac{[\varepsilon]}{[N]^{Re}} = 136 \cdot 6 \text{ eV/\AA}$$

If the ratio of the impurity to Re-atoms is denoted by m/n, the sensitivity of the RBS to the impurity concentration can be predicted as follows /24/:

$$\frac{m}{n} = \frac{H_{imp}}{H_{Re}} \cdot \frac{\sigma_{Re}(E)}{\sigma_{imp}(E)} \simeq \frac{H_{imp}}{H_{Re}} \cdot \left| \frac{Z_{Re}}{Z_{imp}} \right|^2$$

where

H_{imp} and H_{Re} are the peak heights for impurity and Re, respectively,

$\sigma_{imp}(E)$ and $\sigma_{Re}(E)$ are the scattering cross sections for impurity and Re, respectively.

The decrease in film thickness after ion implantation, (if observed)· would be a measure of the sputtering effect. The accuracy of the thickness measurements in this work was ±5%. Figure 3 presents two characteristic RBS spectra of Re-thin films. For films evaporated onto quartz or sapphire, the sensitivity of RBS to nitrogen or oxygen was limited by 5% At. The films grown on carbon substrates increased this detection limit to about 2% At.
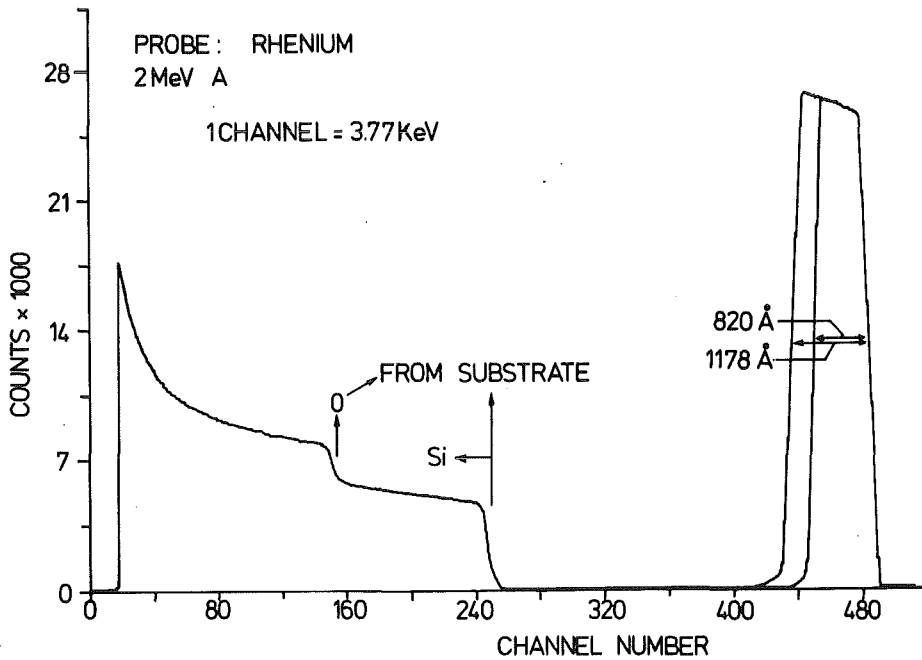
Fig. 3 RBS spectra for 2 MeV He-particles on two Re-films deposited on quartz substrates. Signals from Oxygen and Si are also indicated.

2.4 Resistivity and T_c Measurements:

The specific resistivity at RT, ρ_{RT}, and the specific residual resistivity, ρ_o, were measured by the standard four point method. The voltage drop across 2.5 mm or 5 mm length of the sample was measured for either 100 or 400 μA. The residual resistivity ratio, r, defined as the ratio of the spe-

fic resistances at RT and just before the transition into the superconducting state, was also determined. The r-values are very sensitive to defects or impurities and are considered as a quality factor for the film.

For temperature measurement a Si-diode was used. The reproducibility of temperature measurement was ±0.05 K. The resistive T_c was measured using the standard four-probe method. T_c was also measured inductively. For this purpose a conically shaped primary coil located above the sensor coil, fixed to a sample holder /26/ was used. The sample was placed directly on the sensor coil. The magnetic field of the primary coil is varied by 970 Hz thus inducing a voltage of 1 mV in the sensor coil. As the sample becomes superconducting, the magnetic field is expelled and leads to a reduction of induced voltage in the sensor coil. The amplified signal along with the temperature measured by a Ge-resistor is recorded by an X-Y recorder. To measure a superconducting transition by the inductive method, there must be a set of high T_c fibres which allow a circular current to flow. In contrast for the resistive method only a few high T_c fibres are required along the length of the sample. Generally the value of the inductive T_c was smaller when compared to the resistively measured T_c-values. The inductive T_c is considered to be more representative of a volume effect. T_c is defined here as the temperature at which the resistive or inductive signal has dropped below its normal value by 50%. The transition width ΔT_c was the temperature region in which resistive or inductive signal dropped from 10 to 90%. The lowest temperature attainable in the cryostat was 1.4 K.

2.5 Thin Film X-Ray Diffraction:

Thin film X-ray diffraction measurements were undertaken to determine the phase, lattice parameters, grain size, elastic strains and texture effects in thin films. For this purpose a thin film Guinier camera based on Seemann-Bohlin geometry with the facility of film cassette and a diffractometer was used. One of the significant advantages of using this focusing geometry is that one can use a small angle, γ, between the incident X-ray beam and the surface of the thin film. This increases the effective film thickness by a factor of $1/\sin\gamma$ (neglecting the absorption), thereby decreasing the scattering of the X-rays from the substrate and hence resulting in a decrease of the

background intensity. In this work $\gamma = 10^{\circ}$ was used, i.e. the effective film thickness as compared to the normal incident beam method is increased by a factor of 6.4. The primary X-ray beam which was passed through a Soller slit system was limited by an aperture to a vertical size of 5 mm. X-rays were obtained from a Cu-fine focus tube (8 x 0.1 mm^2) and a Ge-crystal was used as a monochromator. The fine adjustment of the monochromator made it possible to separate $CuK\alpha_1$ and $CuK\alpha_2$ lines. The $CuK\alpha_1$ line with a wavelength of 1.5405 Å was used as the primary beam. The apparatus was calibrated both for photographic as well as diffractometric measurements with an Au-film calibration sample which was evaporated on quartz and was 5000 Å thick with a lattice parameter of nominally 4.078 Å.

The lattice parameters of the rhenium films were determined by a photographic method using an Au standard. A computer programm /27/ has been used to index the X-ray lines and the lattice parameters were determined using the least squares method (LSQ). However, the programm requires information about the crystal structure and approximate values of lattice parameters as input data. The error in the lattice parameters was 0.006 Å.

Different thermal expansion ceofficients of the film and the substrate on which it is grown, introduce thermal stresses in the film resulting from the elastic thermal strains. The information about these strains could be collected using a Seemann-Bohlin geometry. Due to this effect a different value of the lattice parameter is obtained for every reflection (hkl) in case of the cubic structures /28/. In the case of hexagonal structures this information could be extracted from the d-values if the film is considered to be a homogeneous elastic medium. So the maximum strain, ε_ϕ, in a direction at an angle ϕ from the normal to the film is given by /28/

$$\varepsilon_\phi = \varepsilon_1 \cos 2\phi$$

where $\theta = \phi + \gamma$

Now it is assumed that strain components in all the three orthogonal directions are equal and the changes in d-values i.e. $(d_m - d)/d = \Delta d/d$ are plotted against $\cos 2\phi$ where d_m and d are the measured and the calculated d-values, respectively. This plot gives a straight line. The intercept of this line at $\cos 2\phi = -1$ yields the strain ε_1. If ε_1 is negative, the film has compressive strains while for positive value the film has tensile strains. Results of such calculations are shown in Fig. 4. The Re-films grown on quartz have tensile strains. In contrast, films grown on polished sapphire substrates have compressive strains. Thus knowing the Young's modulus, E, of the film material stress, σ, can be calculated by:

$$\sigma_1 = 1.5 \times E \times \epsilon_1$$

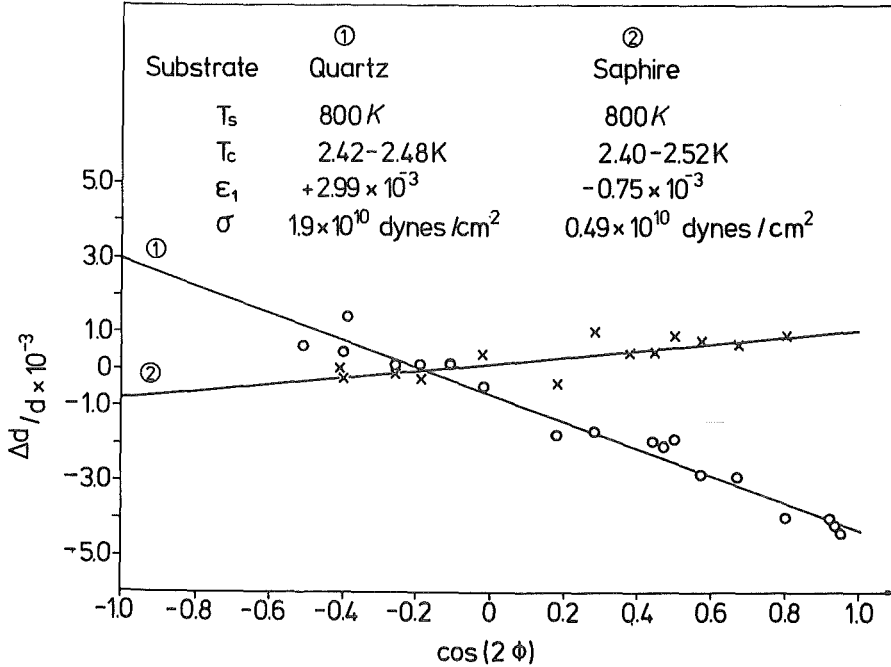| Substrate	① Quartz	② Saphire
T_s	800 K	800 K
T_c	2.42-2.48K	2.40-2.52K
ϵ_1	$+2.99 \times 10^{-3}$	-0.75×10^{-3}
σ	1.9×10^{10} dynes /cm^2	0.49×10^{10} dynes /cm^2

Fig. 4
Effect of thermal strains on the d-values of Re films evaporated on to quartz and polished sapphire.

The crystallite size, D was determined from X-ray line broadening using the formula of Scherrer /29,30/.

$$D = K\lambda/(\beta-b) \cos \theta$$

K is a constant approximately equal to unity and depends on the crystallite shape; β is the full width at half maximum of the X-ray line; b is the width of the line broadening produced under similar geometrical condition by the same material with a crystallite size well above 1000 Å. Here b was taken as zero; θ is Bragg's angle; and λ is the X-ray wavelength. For both the polished and rough substrates, the broadening of each X-ray line was used to calculate the crystallite size. The average value obtained is denoted by $\bar{D}$.

Intensities of the X-ray lines were measured with the diffractometer. The intensity of the Au-standard was used for control. The spectrum was registered in a multichannel analyser which allows for automatic peak integration. A linear background correction was also applied. The integrated peak area gave the intensity.

2.6 Annealing Experiments:

Annealing experiments were performed in an evacuated steel tube at pressure of around 10^{-7} Torr. A movable ceramic tube oven, heated up to the desired temperature was then moved over the steel tube in which the sample had been placed. Just before shifting the oven over the steel tube, the vacuum was 5×10^{-7} Torr and depending on the annealing temperature rose to 10^{-6} Torr. The highest annealing temperature was 1473 K which was measured by a thermocouple. The annealing experiments were isochronal and samples were annealed every time for 30 minutes at a given temperature.

3. Results:

3.1 Thin Film Properties:

The electrical and superconducting properties of the Re-films along with their crystallographic phase and lattice parameters were determined as a function of preparation parameters such as rate of evaporation, R, pressure in evaporation chamber, p, substrate material (quartz, sapphire, carbon), substrate temperature, T_s, annealing temperature, T_A, substrate surface (rough or polished) and film thickness, t.

3.1.1 Influence of Preparation Parameters:

3.1.1.1 Evaporation Rate and Pressure:

To investigate the influence of the above mentioned parameters on resistivity, T_c and structure of evaporated films a systematic procedure was adopted. Each time only one parameter was varied and all others were kept constant. Table 3 shows the properties of films evaporated at R-values between 1 and 20 $\overset{o}{A}$/sec by keeping t, p and T_s constant. Similarly Table 4 shows the resistivity, T_c and structure of the films for which only p was varied between 10^{-8} and 10^{-5} Torr.

Table 3

Films evaporated onto polished sapphire and quartz with t = 1500 $\overset{o}{A}$, T_s = 900 K and p = 10^{-7} Torr as a function of R.

sub-strate	R $\overset{o}{A}$/sec	Lattice parameters		$V_c[\overset{o}{A}^3]$	Resistivity [μΩcm]		r	resistive $T_c[K]$	$\Delta T_c[K]$
		a[$\overset{o}{A}$]	c[$\overset{o}{A}$]		ρ_{RT}	ρ_0			
Polished sapphire	1.1	2.761	4.461	29.451	21.2	3.7	5.7	2.08	0.21
	2.5	2.762	4.462	29.479	21.0	4.6	4.6	2.27	0.15
	5.1	2.761	4.456	29.418	19.0	5.1	3.7	2.06	0.20
	6.7	2.762	4.457	29.446	22.0	6.0	3.7	2.20	0.20
	9.0	2.761	4.456	29.417	18.0	4.5	4.0	2.18	0.26
	13.6	2.764	4.458	29.495	19.2	5.8	3.3	2.16	0.08
	20.5	2.766·	4.450	29.484	20.5	6.2	3.3	2.19	0.14
Quartz	1.5	2.758	4.463	29.400	22.9	4.9	4.7	2.35	0.24
	4.2	2.763	4.461	29.493	24.5	6.5	4.1	2.30	0.40
	6.8	2.763	4.459	29.480·	22.8	5.3	4.3	2.10	0.21
	12.9	2.766	4.450	29.485	25.0	5.0	5.0	2.25	0.30
	18.0	2.764	4.462	29.522	23.4	5.2	4.5	2.21	0.27

Table 4

Films evaporated as a function of pressure in vacuum chamber, p on quartz and sapphire, at T_s = 900 K, R = 3 Å/sec and t = 1500 Å.

substrate	p Torr	Lattice parameters		V[Å³]	Resistivity [μΩcm]		r	resistive T_c[K]	ΔT_c[K]
		a[Å]	c[Å]		ρ_{RT}	ρ_o			
Polished sapphire	1.10^{-5}	2.759	4.464	29.428	23.0	4.6	5.0	2.25	0.10
	3.10^{-6}	2.759	4.465	29.434	22.7	4.9	4.6	2.00	0.20
	5.10^{-6}	2.760	4.463	29.443	21.2	4.7	4.5	2.30	0.25
	1.10^{-7}	2.762	4.458	29.452	24.1	5.3	4.5	2.19	0.18
	1.10^{-8}	2.763	4.459	29.480	21.5	4.1	5.2	2.21	0.19
Quartz	1.10^{-5}	2.764	4.462	29.521	24.4	4.3	5.7	2.23	0.17
	1.10^{-6}	2.763	4.463	29.507	19.8	5.2	3.8	2.31	0.25
	1.10^{-7}	2.761	4.458	29.431	25.6	5.8	4.4	2.18	0.20
	5.10^{-7}	2.766	4.450	29.485	23.2	4.9	4.7	2.21	0.15
	1.10^{-8}	2.762	4.458	29.452	22.4	5.5	4.1	2.25	0.23

Variations of R and p in the above mentioned range, did not affect either the resistivity at RT, ρ_{RT}, T_c or the structure. However, it can be seen that the values of ρ_{RT} and T_c obtained here are somewhat larger than the bulk Re which has a ρ_{RT} value of 18.0 μΩcm and T_c-value of 1.7 K.

3.1.1.2 Substrate Material:

As a next step the influence of substrate materials on film proper-ties was studied. In general the films grown on quartz were not stable and cracked after a few hours depending on the film thickness. Typical resistive T_c-values of 2.2 to 2.6 K and ρ_{RT}-values of 22 - 27 μΩcm were observed. Films grown on polished sapphire substrates at T_s below 650 K were also unstable and cracked at RT, 2 to 3 hours after their formation. For these films re-sistive T_c-values of 2.9 to 3.3 K and ρ_{RT}-values of 65 to 70 μΩcm were re-gistered. These observations are in agreement with the work of Frieberthauser et al. /1/. Due to this instability, the films grown below 650 K could not be analysed further.

A strong influence of the substrate material on the elastic strains in the films was noted. When an evaporated film and the substrate on which the film is grown have different thermal expansion coefficients, changing the temperature of the combination will introduce elastic strains in the

films. Due to this effect a different value of the lattice parameters is obtained for every reflection (hkl) in the Seemann-Bohlin geometry /28/. This analysis showed that films on sapphire have compressional strains while those grown on quartz have tensile strains. Films on quartz have a stress value on the order of 10^{10} dynes cm^{-2} which is four times larger than the films grown on sapphire (Fig. 4). As mentioned above, the films on quartz are not stable. High strains in these films may cause this instability.

Dependence of ρ_{RT}, ρ_o or T_c on these strains was not observed. From literature data /30/ it can be estimated that for Re a pressure which corresponds to elastic strains would lead to a decrease in T_c of 0.1 K. Thus it may be concluded that the strains in these films are not responsible for the observed high T_c-values.

3.1.1.3 Impurities:

Impurities are known to effect the physical properties of thin films. Thus a knowledge of the impurity content is very important. RBS on the Re films showed that heavy elements (Z $\geq$ 15) were not present in the detection limit of <±1 at%. On a few randomly selected films proton induced X-ray emission measurements were undertaken. The results confirmed the findings of RBS and no traces of heavy elements (Z > 11) on the order of parts per million could be detected. RBS showed that the oxygen and nitrogen content in films was below 2 at%. The influence of oxygen on the electrical and superconducting properties of the Re-films was further studied on films grown in an oxygen atmosphere of 10^{-5} Torr at 900 K. RBS showed that these films had 6 at% oxygen. However, no significant difference was found in the ρ_{RT}, T_c and lattice parameters of these films as compared with those grown without oxygen.

There is little probability that nitride or oxide of rhenium may form above 900 K. This is due to the fact that rhenium nitride /31/ and rhenium oxide /32/ decompose at 553 K and 825 K, respectively. No rhenium carbide has been observed until now /33/. Hence it may be concluded that the high values of ρ_{RT} and T_c as compared to the bulk Re in the above mentioned films are not due to impurities but, as will be discussed later, could be due to intrinsic defects produced during film growth or cooling to RT.

3.1.1.4 Substrate Temperature:

The film quality was considerably improved by increasing the substrate temperature. This is obvious from Fig. 5 where the residual resistivity ratio, r is plotted as a function of substrate temperature for polished and rough substrates. The value of r increases for both polished and rough substrates as T_s is increased from RT to 1330 K. A larger increase in the r-values is observed for polished substrates and a value of 22.0 is obtained as compared to 7.8 for rough substrates at $T_s \simeq 1330$ K. Therefore, it may be concluded from Fig. 5, that the films grown on polished substrates will have fewer defects than those deposited onto rough substrates.
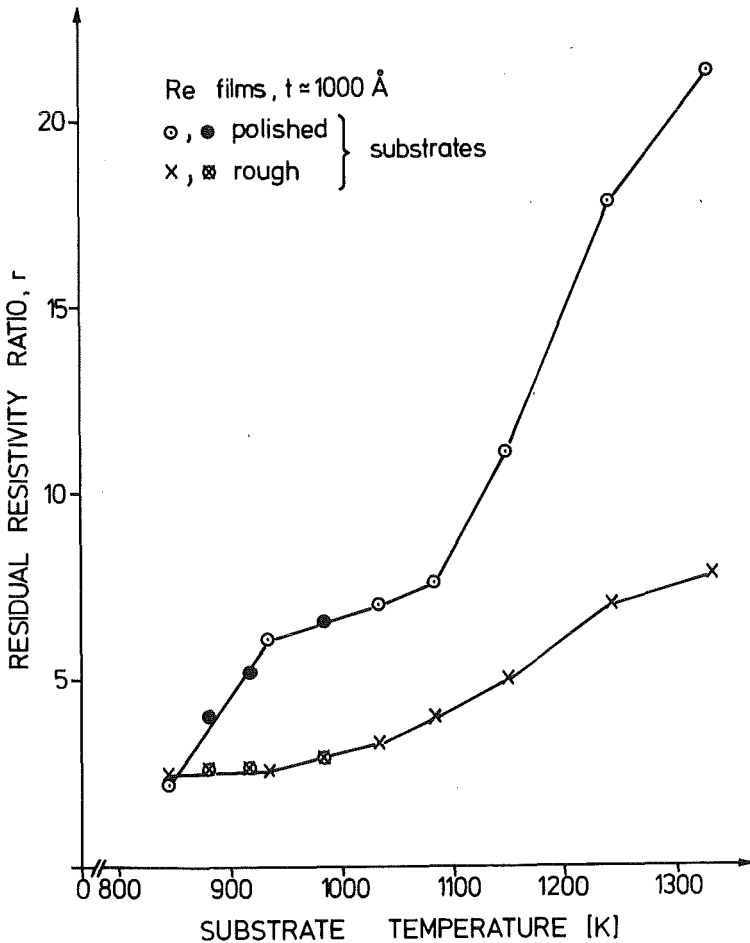

Fig. 5
Residual resistivity ratio as a function of substrate temperature for 1000 Å thick Re-films grown on polished and rough substrates. r-values for two sets of films are plotted in each case.

In Fig. 6 the residual resistivity, ρ_o, as a function of T_s is shown for polished and rough substrates. The values of ρ_o are observed to decrease with increasing T_s. For rough substrates, ρ_o-values are higher than those for polished substrates. Figure 6 also presents the values of thermal part of resistivity,

Fig. 6
Residual resistivity ρ_o as a function of substrate temperature for films grown on polished and rough substrates. Two sets of films in each case are plotted. Thermal part of resistivity as a function of T_s is also presented.
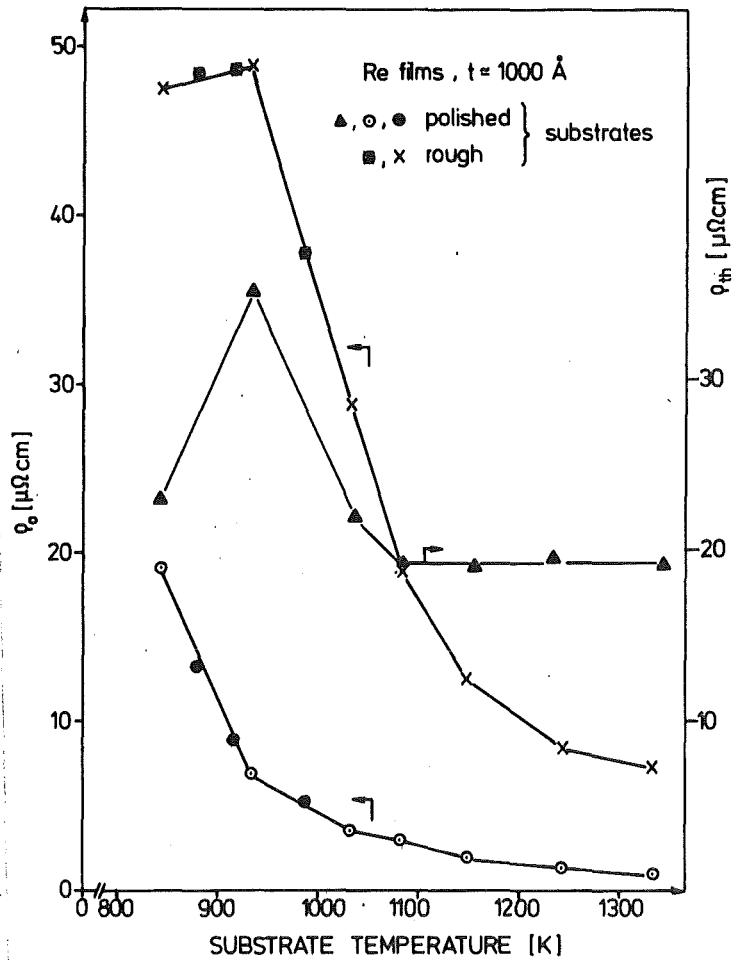
ρ_{th}, as a function of T_s where ρ_{th} is the difference between ρ_{RT} and ρ_o. The values of ρ_{th} appear to be constant above 1090 K i.e. Matthiesen rule is violated for films evaporated onto polished substrates at T_s < 1090 K.

In Fig. 7 the superconducting transition temperature is plotted for polished and rough substrates as a function of T_s. Here the T_c-values of different charges are in good agreement. Since the resistively measured T_c-values for rough- and polished-substrates are approximately the same and show the same functional dependence on T_s, only those for the polished substrates are plotted. A resistive T_c-value of 2.7 K is obtained for $T_s \simeq 850$ K which decreased and reached a value of 1.7 K at 1330 K. Irrespective of the substrate surface, bulk T_c-values are always obtained at high substrate temperatures. At low substrate temperatures inductive T_c values are higher for polished surfaces. As will be discussed later, this may be due to the homogeneous distribution of the vacancies in this case. For rough substrates the transition temperature width is broader than for polished substrates indicating a rather inhomogeneous distribution of regions with enhanced T_c-values.
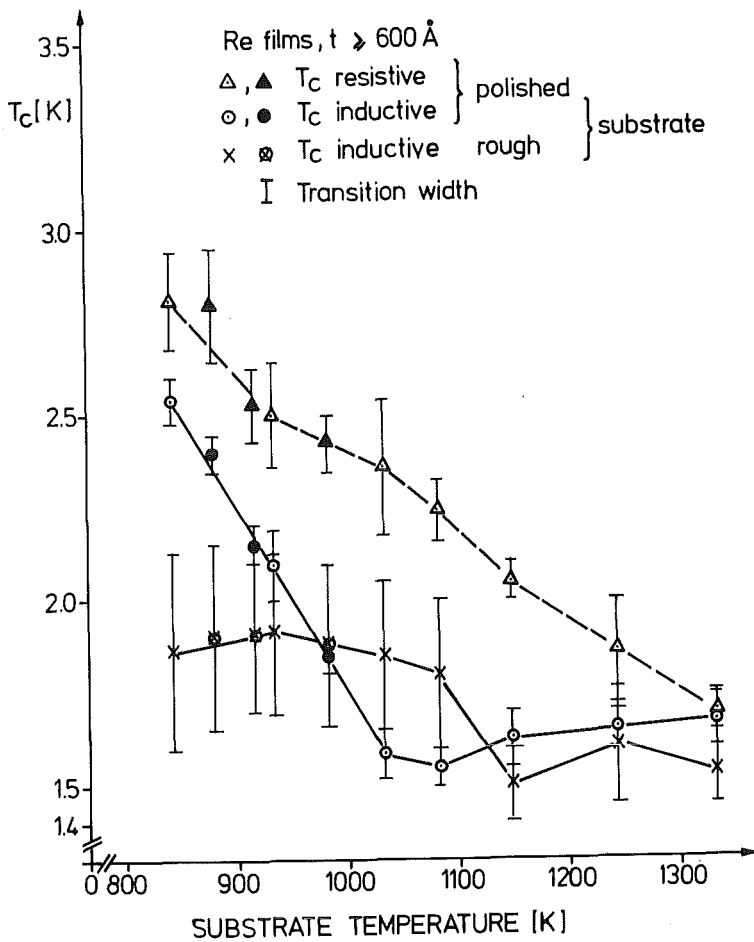
Fig. 7
Inductively - and resistively -
measured T_C of Re-films as a
function of substrate temperature.
Inductive T_C-values are shown for
films grown on both, polished and
rough substrates. Again two
sets of films in each case are
plotted to show the reproducibi-
lity of the results.

3.1.1.5 Structure:

The structure of the films was also investigated as a function of T_s.
The films grown on polished sapphire substrates above 1000 K showed

texture effects. At 1330 K nearly single-crystalline films with

crystallite orientation in [0001] direction is obtained. The number of X-ray

lines was found to decrease with increasing T_s. At 700 K, 12 X-ray lines are

detected, whereas between 1150 and 1330 K only 2 to 3 X-ray lines are observed.

Above 1150 K the lattice parameters could not be determined due to the absence

of a sufficient number of X-ray lines. All films evaporated either on quartz

or sapphire revealed the hcp Re-structure with lattice parameters and cell

volume slightly above the bulk material. Table 5 shows the lattice parameters

and cell volume as a function of T_s for films evaporated onto polished and

rough substrates. No dependence of lattice parameters or cell volume on T_s is

noted.

Table 5

Lattice parameters and cell volume of Re-hcp phase as a function of T_s for films grown on polished and rough substrates. For polished substrates lattice parameters above 1100 K could not be determined.

Substrate Temperature	Polished Substrates			Rough Substrates		
T_s [K]	a[Å]	c[Å]	V_c [Å^3]	a[Å]	c[Å]	V_c [Å^3]
850	2.759	4.465	29.434	2.763	4.454	29.447
920	2.778	4.459	29.801	2.767	4.465	29.605
1030	2.758	4.466	29.420	2.765	4.464	29.556
1090	2.767	4.475	29.672	2.762	4.465	29.498
1150	-	-	-	2.763	4.469	29.546
1240	-	-	-	2.764	4.465	29.541
1330	-	-	-	2.761	4.463	29.464

Since the films on polished substrates showed texture or single-crystalline structure above 1000 K, films were also grown on rough substrates as a function of T_s so as to obtain polycrystalline films at high T_s-values. These films always showed 16 X-ray lines from Re-hcp phase together with 4 to 5 X-ray lines of a new phase. At T_s between 1150 and 1330 K the number of lines which did not belong to Re-hcp phase increased to 8, thereby indicating that high substrate temperature favours the formation of a new phase which most probably is a χ-phase and belongs to Al_5Re_{24} /34/. This phase is formed by the reaction of Re with the sapphire substrate. Intensity measurements of X-ray lines give a rough idea about the quantity of this phase. The amount of Al_5Re_{24} phase increased from 1 to 7% (compared to Re) as T_s was increased from 850 to 1330 K. The changes in lattice parameters and cell volume in this case also do not depend on T_s (Table 5).

The average crystallite size $\bar{D}$ as a function of substrate temperature is presented in Table 6 together with the values of residual resistivity and inductively measured T_c. A slight increase of $\bar{D}$ with increasing substrate temperature is noted. At low T_s there exists a difference in crystallite size between rough and polished substrates which seems to correlate with the different ρ_o values. This correlation, however, does not exist at high T_s-values indicating that ρ_o is not determined by grain size even at low T_s. This will be discussed further below.

Table 6

The crystallite size, residual resistivity, inductive superconducting transition temperature for polished- and rough-substrates as a function of substrate temperature.

T_s[K]	Average crystallite size, $\bar{D}$[Å]		Residual resistivity ρ_o [$\mu\Omega$cm]		Inductive T_c[K]	
	polished	rough	polished	rough	polished	rough
850	275	362	19.1	47.5	2.48-2.60	1.60-2.13
920	294	472	6.9	48.9	2.00-2.19	1.70-2.13
1030	410	427	3.5	28.8	1.52-1.65	1.65-2.05
1090	404	491	2.9	18.9	1.50-1.60	1.60-2.00
1150	325	548	1.9	12.5	1.55-1.70	1.40-1.60
1240	s.c.	487	1.3	8.4	1.60-1.70	1.45-1.76
1330	s.c.	559	0.9	7.3	1.60-1.75	1.45-1.60

s.c.: single-crystalline film

3.1.1.6 Annealing Experiments on as Grown Films:

In order to determine the type of defect responsible for high values of T_c and ρ_o, isochronal annealing experiments were performed on films evaporated onto polished and rough substrates at 700 K. Figure 8 shows the inductive T_c values as a function of annealing temperature, T_A. No recovery is observed up to 600 K as expected. For polished substrates recovery is noted at about 0.20 T_m and 0.27 T_m (T_m - melting point for Re: 3453 K). With increasing annealing temperature the transition width increased from about 0.20 K to 0.65 K at 0.22 T_m and decreased to 0.30 K at 0.31 T_m. For rough substrates no significant recovery stages are observed and at 700 K (0.20 T_m) T_c-values similar to bulk values are noted.

The annealing stages as observed here in an isochronal annealing process, are in agreement with those determined during film growth at various substrate temperatures (Fig. 7). Referring to the literature on either fcc or hcp metals /35/, the peaks at 0.20 T_m and 0.27 T_m correspond to stage IV and stage V, respectively. The stage IV belongs to the small vacancy clusters which disappear in favour of larger ones, while stage V is attributed to the annealing of dislocation loops accompanied with the break up of defect clusters.
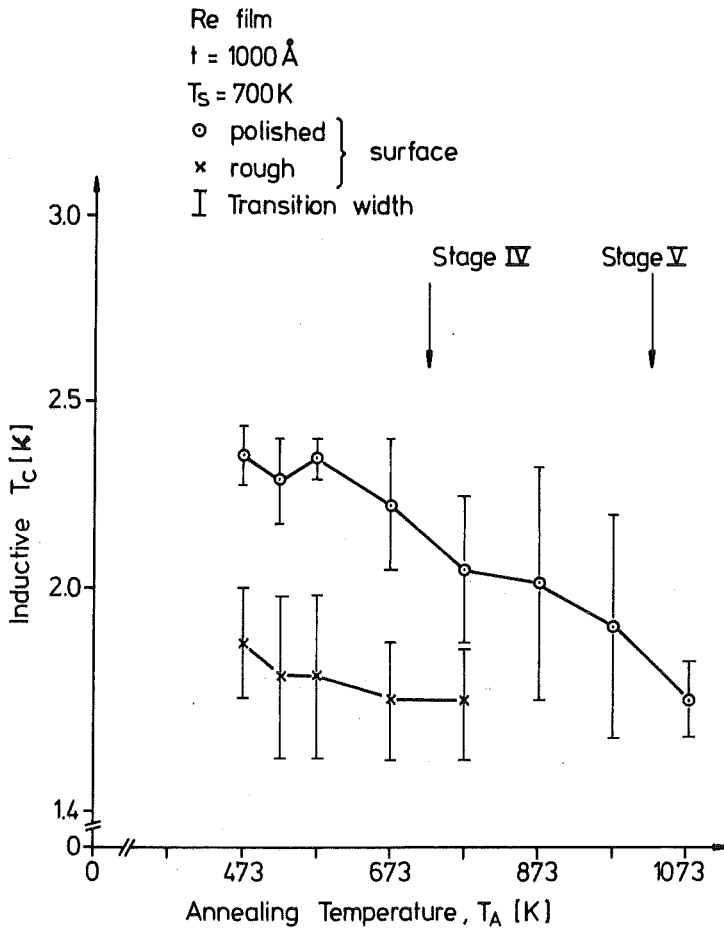
Re film
t = 1000 Å
T_S = 700 K
⊙ polished ⎱
× rough ⎰ surface
I Transition width

Fig. 8
Inductively measured T_C of
Re films grown at 700 K on
polished- and rough sub-
strates as a function of
annealing temperature.
Notation of stages IV and
V is adopted after Ref. /35/.
The vertical bars, I, are T_C-
transition widths.

3.1.2 Thickness Dependence of T_C and ρ :

The thickness dependence of resistivity and T_C was studied for the films grown on polished sapphire substrates only. The films evaporated at 900 K were always poly-crystalline while those evaporated at 1330 K had single-crystalline structure.

3.1.2.1 T_C as a Function of Film Thickness:

As mentioned earlier the films grown at high substrate temperatures have ρ and T_C values comparable to the bulk material. Therefore these films are suitable for studying the thickness dependence of T_C and ρ. The residual resistivity ratio, r of these films was in the range of 2 to 15 as the film thickness varied from 190 Å to 840 Å.
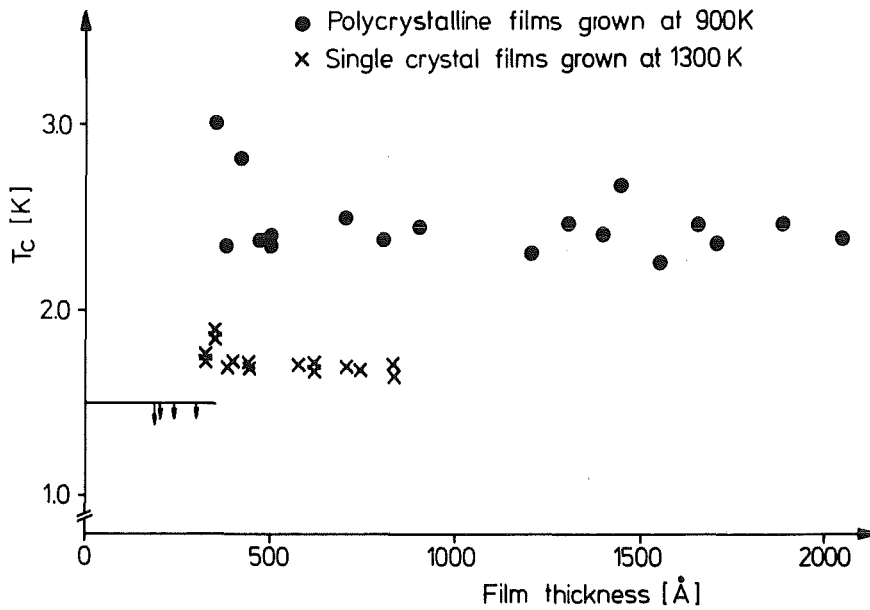
Fig. 9   Resistively measured T_C of polycrystalline and single-crys-
talline films as a function of film thickness. Lowest tem-
perature attainable in the cryostât was 1.4 K, which is
indicated by the solid line.

Figure 9 shows the resisitve T_c as a function of film thickness for
polycrystalline films grown at 900 K and single-crystalline films grown at
1300 K. For single-crystalline films, no significant difference between in-
ductive and resistive T_c was noted above 450 Å and a T_c-value comparable to
the bulk value is obtained. The T_c-values   show   a slight increase in the
film thicknesses between 300 and 400 Å. Below 300 Å, no T_c is observed
until 1.4 K is reached.

The higher values of T_c for a constant value of the thickness for poly-
crystalline films may be due to a large number of defects as compared to the
single-crystalline films. These films also show an increase in T_c in the
film thickness region of 300 to 400 Å but below 300 Å, no T_c is observed. The
transition width ΔT_c for film thicknesses above 500 Å was 0.24 K to 0.32 K as
compared to films below 500 Å where it was between 0.2 K and 0.6 K for poly-
crystalline and single-crystalline films.

3.1.2.2 Determination of Mean Free Path of Conduction Electrons, l_o:

The successful preparation of nearly single-crystalline Re films grown on polished substrates with bulk properties allowed to study the influence of film thickness on resistivity and to obtain information on the mean free path of the conduction electrons, l_o, in Re. It is well known that as the thickness, t, of a metal film becomes comparable in magnitude to l_o, the film boundaries impose a geometrical limitation called size effect, on the motion of the conduction electrons /36/. The size effect theory of Fuchs /37/ and Sondheimer /38/ leads to the following equations for two limiting cases /36/;

(1)   For $t \geq l_o$

$$\rho_F = \rho_B + \{0.375 \rho_B K^{-1} (1-P)\}$$

(2)   For $t \ll l_o$

$$(\rho_F t)^{-1} = 0.75 \{(1+P)/(1-P) l_o \rho_B\} \{(\ln l_o + 0.4228) - \ln t\}$$

where ρ_B = resistivity of the bulk material; P = specular scattering factor (P is zero for complete diffuse scattering) and $K = t/l_o$ (ratio of the film thickness to mean free path). The condition $t \geq l_o$ is normally satisfied for resistivity values at RT whereas measurements of resistivity on the same films at LNT (77.3 K) and LHeT (4.2 K) fulfill the condition $t \ll l_o$.

A further possible method of determining the product $l_o(1-P)$ is to use the temperature coefficient of resistivity (TCR). Knowing that the resistivity in this case shows a linear dependence in the temperature region between RT and LNT, TCR is defined as given in Ref. /1/.

$$\alpha = d\rho / (\rho_{LNT} \cdot dT)^{\circ}C,$$

$$= (\rho_{RT} - \rho_{LNT}) / (\rho_{LNT} \cdot 222)^{\circ}C.$$

The following expression for TCR is used to analyse the data /36/:

(3) $\alpha_F = \alpha_B \{1 - 0.375 (1-P) K^{-1}\}$

            for $t \geq l_o$

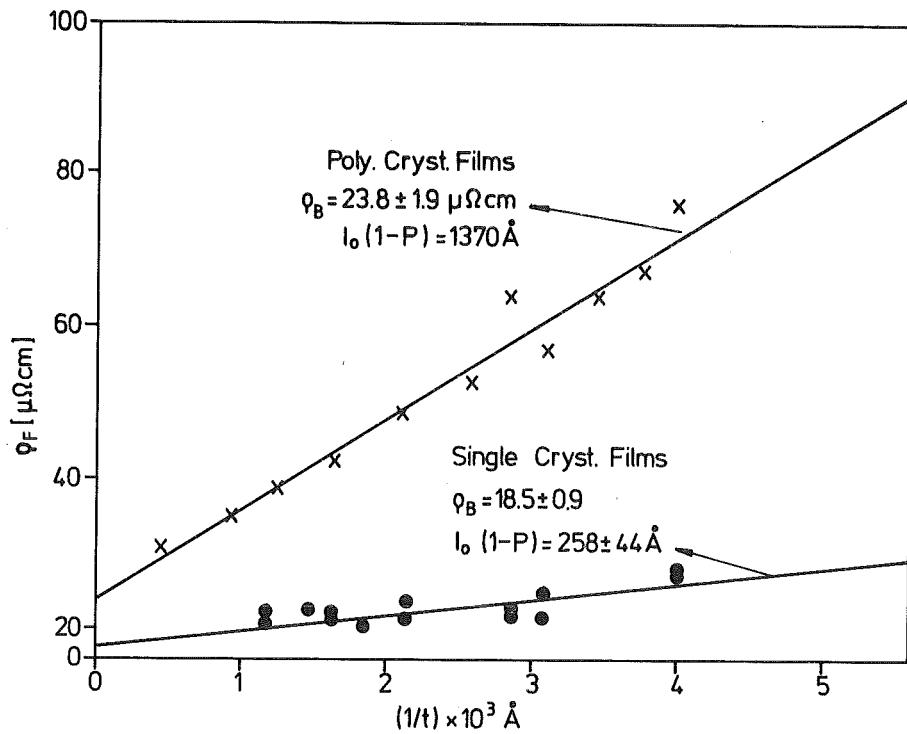where α_F and α_B are TCR for films and bulk material, respectively.

Fig. 10 RT-resistivity versus reciprocal film thickness of poly-
crystalline and single-crystalline films. Solid lines
are rms - fits to the measured data.

In order to analyse the data for the thickness dependence of the re-
sistivity, the films with thicknesses smaller than 250 Å have been ignored
due to the fact that these cannot be considered as homogeneous films of con-
stant thickness. They are films whose thickness varies around a mean value.
The regions of small thicknesses would lead to a high value of resistivity.
This is in accordance with previous work /39/. Figure 10 shows
the changes in film resistivity as a function of 1/t for single-crystalline
films. For comparison the values of ρ_F for a set of polycrystalline films
are also plotted in Fig. 10. The LSQ method is used to fit equation 1 and
the following values are obtained:

	$\rho_B [\mu\Omega cm]$	$l_o (1-P) [Å]$
Polycrystalline films	23.8 ± 1.9	1370 ± 42
Single-crystalline films	18.5 ± 0.9	258 ± 44

The ρ_B-value obtained from single-crystalline films is in agreement
with the bulk value of Re. The polycrystalline film data resulted in a higher

value of ρ_B. From this comparison it may be concluded that for such an analysis only single-crystalline films should be used. The slope of the straight line in Fig.10 gives the product of $l_o(1-P)$ i.e. with two unknown parameters l_o and P. The product $l_o(1-P)$ can also be determined using equation 3 and applying the LSQ method. Here a value of 360 ± 65 Å is obtained for single-crystalline films which is in good agreement with the above mentioned value.

Equation 2 makes it possible to determine the value of l_o and P separately. The data for resistivity measured on the same films at LNT are analysed again by the LSQ method. A straight line is fitted for a plot of $(\rho_F t)^{-1}$ versus $\ln(t)$. The ratio of the axis intercept to the slope of the line gives the value of 2240 ± 403 Å for l_o (LNT). Knowing l_o at LNT, P can be calculated as 0.81 ± 0.04. The resistivity values at LNT and LHeT are plotted in Fig. 11 as a function of film thickness. Solid curves are drawn using l_o and P values which showed the best fit for the LNT data.
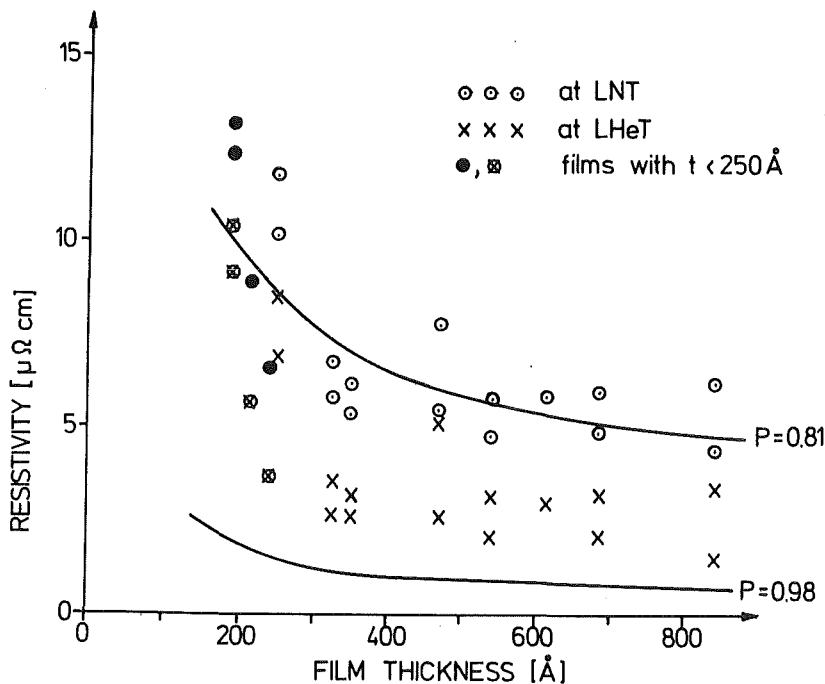

Fig. 11
Thickness dependence of resistivity, measured at LNT and LHeT. Solid lines are rms - fits to the measured data. Films having thicknesses smaller than 250 Å have not been included for rms - fit.

The analysis of ρ_{LHeT} data using equation 2 yields an l_o(LHeT) value of 5494 ± 2000 Å and a value of 0.98 ± 0.01 for P. This low value of l_o(LHeT) as compared to values given in Ref. /40/ is due to the strong influence of defects on the resistivity values especially at low temperatures. Fig. 11 also shows that the values of l_o and P calculated from LHeT data do not give the

best fit for the measured resistivity values. The disagreement shows that the influence of the film thickness is insufficient to explain the high resistivity values at LHeT and may be due to defects /36/ in these films.

Thus as will be shown later on the l_o-value for Re at LNT is 2240 ± 403 Å while at RT this value lies between 258 and 360 Å. The l_o-value at LHeT could not be estimated by this method. This will be further discussed in chapter 4.

Due to the fact that l_o(RT) for Re lies between 258 to 360 Å, the films used for ion irradiations and implantation studies had always thicknesses greater than 500 Å. In this way the influence of size effects on the resitivity was avoided.

3.2 Ion Induced Intrinsic Defects:

In order to produce ion induced intrinsic defects, Re-films evaporated onto polished substrates were used. Thirty Re films with poly- and single-crystalline structures were irradiated with 700 keV Ar-ions at RT and LNT and 350 keV N-ions at RT. Table 7 presents the pre-irradiation properties of eight polycrystalline films. Inductive T_c-values for these films were between 1.8 to 2.0 K. The single-crystalline films had ρ_{RT}-values of 18 to 19 μΩcm and r-values between 15 and 20. For these films inductive and resistive T_c-values were similar and on the order of 1.8 K. The results of ion irradiations on the above mentioned films are presented below:

Table 7

The pre-irradiation properties of poly-crystalline Re films

S.No.	Thickness [Å]	Resistivity [μΩcm]		r	T_c[K] *	ΔT_c[K]	Lattice param.		V[Å³]	conditions for ion irradiation
		ρ_{RT}	ρ_o				a[Å]	c[Å]		
1	1047	21.3	4.0	5.3	2.46	0.12	2.762	4.458	29.458	N-ions at RT
2	1400	19.8	1.8	11.0	2.67	0.06	2.760	4.480	29.560	—— do ——
3	1360	21.4	4.2	5.1	2.15	0.15	2.761	4.461	29.459	—— do ——
4	1180	20.3	3.3	6.2	2.16	0.16	2.763	4.460	29.500	—— do ——
5	1200	19.5	2.5	7.8	2.06	0.14	2.762	4.465	29.519	Ar-ions at RT
6	1150	22.7	5.5	4.1	2.20	0.10	2.764	4.470	29.583	—— do ——
7	740	20.4	3.1	6.6	1.90	0.10	2.763	4.459	29.502	—— do ——
8	1000	19.8	2.3	8.6	2.24	0.04	2.754	4.480	29.448	—— do ——

* T_c values were resistively measured. Inductive T_c-values were between 1.8 to 2.0 K.

3.2.1 Influence of Ar-Ion Irradiation:

To compensate for the different pre-irradiation ρ_o-values (Table 7), the ion induced residual resistivity, $\Delta\rho_o$, is obtained by subtracting pre-irradiation values from the post-irradiation values i.e. $\Delta\rho_o = \rho_o(\phi) - \rho_o(\phi = 0)$ where ϕ is the fluence. Fig. 12 shows the $\Delta\rho_o$-values as a function of ϕ for RT-irradiated films. The values for four different films show good agreement although the pre-irradiation ρ_o-values were 0.6, 4.1, 6.6 and 7.8 $\mu\Omega$cm. Thus it may be concluded that $\Delta\rho_o$ as a function of ϕ does not depend on the pre-irradiation ρ_o-values and the crystalline structure of the film.
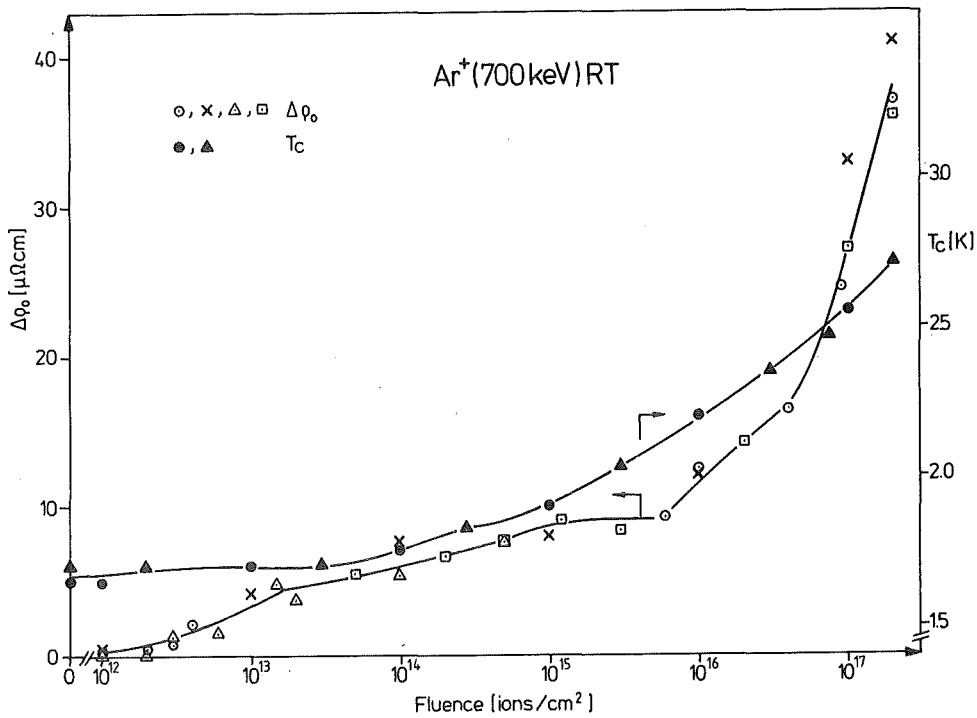

Fig. 12 The changes in $\Delta\rho_o$- and T_C- as a function of Ar-ion fluence. The $\Delta\rho_o$ values for 4 different films and the T_C-values for 2 different films with poly- and single-crysatalline structures are plotted.

3.2.1.1 Ion Induced $\Delta\rho_o$ and T_c:

In Fig. 12 it can be seen that $\Delta\rho_o$ increases as a function of ϕ and seems to saturate in the fluence region between 1 x 10^{15} and 6 x 10^{15} Ar-ions/cm^2 at a value of 9 $\mu\Omega$cm. For higher fluences a further rapid increase of $\Delta\rho_o$ is

noted and a value of 37 $\mu\Omega$cm is obtained for 2×10^{17} Ar-ions/cm^2. Further irradiation caused macroscopic damage of the film.

The fluence dependence of $\Delta\rho_o$ seems to reflect the production of two different types of defect structures. The first type of defect structure is produced mainly at low fluences and seems to saturate above 1×10^{15} Ar-ions/cm^2. The second type of defect structure is mainly produced by fluences above 6×10^{15} Ar-ions/cm^2. From the initial slope $d\Delta\rho_o/d\phi$ (Fig. 13) for the first type of defect structure, the number of Frenkel pairs, N_F, can be estimated by the relation /41/:

$$N_F = n \cdot t (d\Delta\rho_o/d\phi) \cdot \rho_F$$

where t is the film thickness, n is the number of Re atoms/cm^2 and ρ_F is the resistivity per unit concentration of Frenkel pairs ($\rho_F = 2 \times 10^{-3}$ Ωcm for Re /21/). The value for N_F, which is about 132 Frenkel pairs per incident ion, can be compared to a value of 682 which is estimated using the Kinchin and Pease model /42/ where $N_F = \varepsilon(T_a \cdot C)$ with $\varepsilon = 90$ keV /43/, c = 3.3 and T_a is the threshold energy which is 40 eV for Re/21/. About 81% of the Frenkel pairs anneal out in stage I (up to 350 K) so that only 19% still remain. These calculations are true for C = 3.3. For increasing cascade production /43/ the number of Frenkel pairs surviving stage I would be further decreased to 12% as value of C would take the classical value of 2.

The second type of defects seems to be produced at fluences above 6×10^{15} Ar-ions/cm^2. The sharp increase of $\Delta\rho_o$ in this fluence region, however, could also be attributed to sputtering or ion beam mixing with the substrate atoms. These $\Delta\rho_o$-values have already been corrected for the sputtering effect, whether these values could be attributed to ion beam mixing is the only remaining question. RBS measurements did not reveal any mixed layer at the interface with thicknesses above 200 $\overset{o}{A}$. Therefore ion beam mixing with the substrate can be excluded. It is assumed that the large increase of $\Delta\rho_o$-values is due to the formation of extended defects such as dislocations. Schultz /44/ has observed a large value of 6.7×10^{-17} Ωcm^3 per dislocation/cm^2 in Re. From the slope of a plot $\Delta\rho_o - \Delta\rho_o^{sat}$(I) vs. ϕ, (Fig. 14) which is 1.3×10^{-22} Ωcm^3, using both these values the production rate of 1.9×10^{-6} dislocations/ion is estimated. Thus the areal density of dislocations lies between 1.2×10^{10} and 4×10^{11} for fluences between 6×10^{15} and 2×10^{17} ions/cm^2. Dislocation densities of this magnitude are usually observed after a high dose of ion implantation /45/. The increase in $\Delta\rho_o$ as a function of ϕ for Ar-ions irradiation at LNT (Fig. 15) shows no difference when compared with RT-irradiations.

Fig. 13
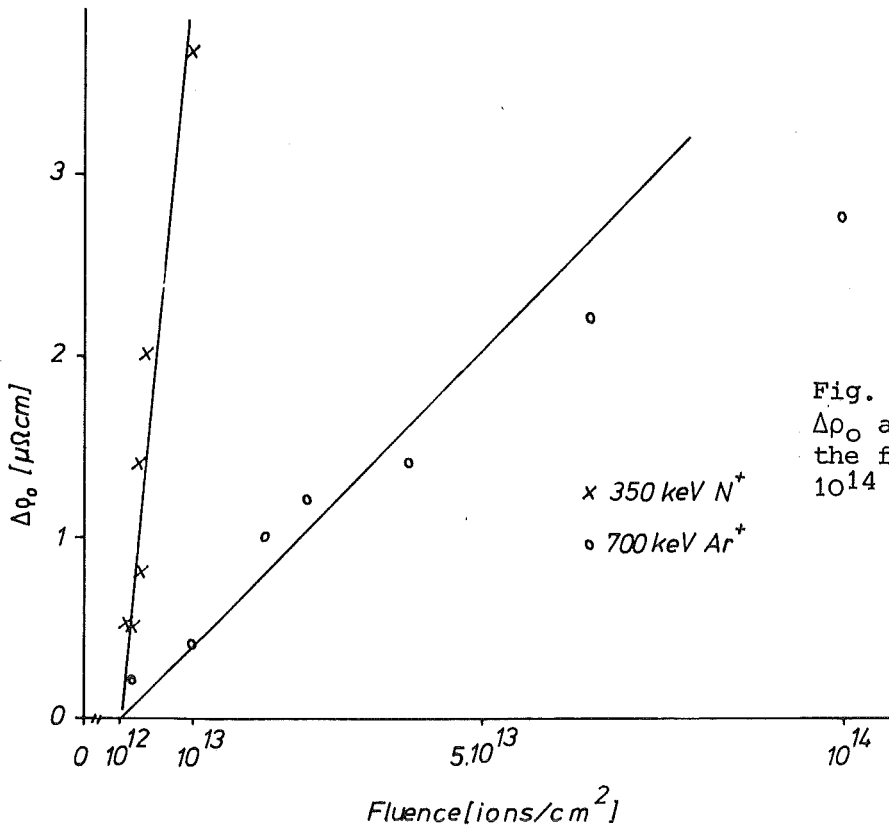$\Delta\rho_0$ as a function of ϕ for
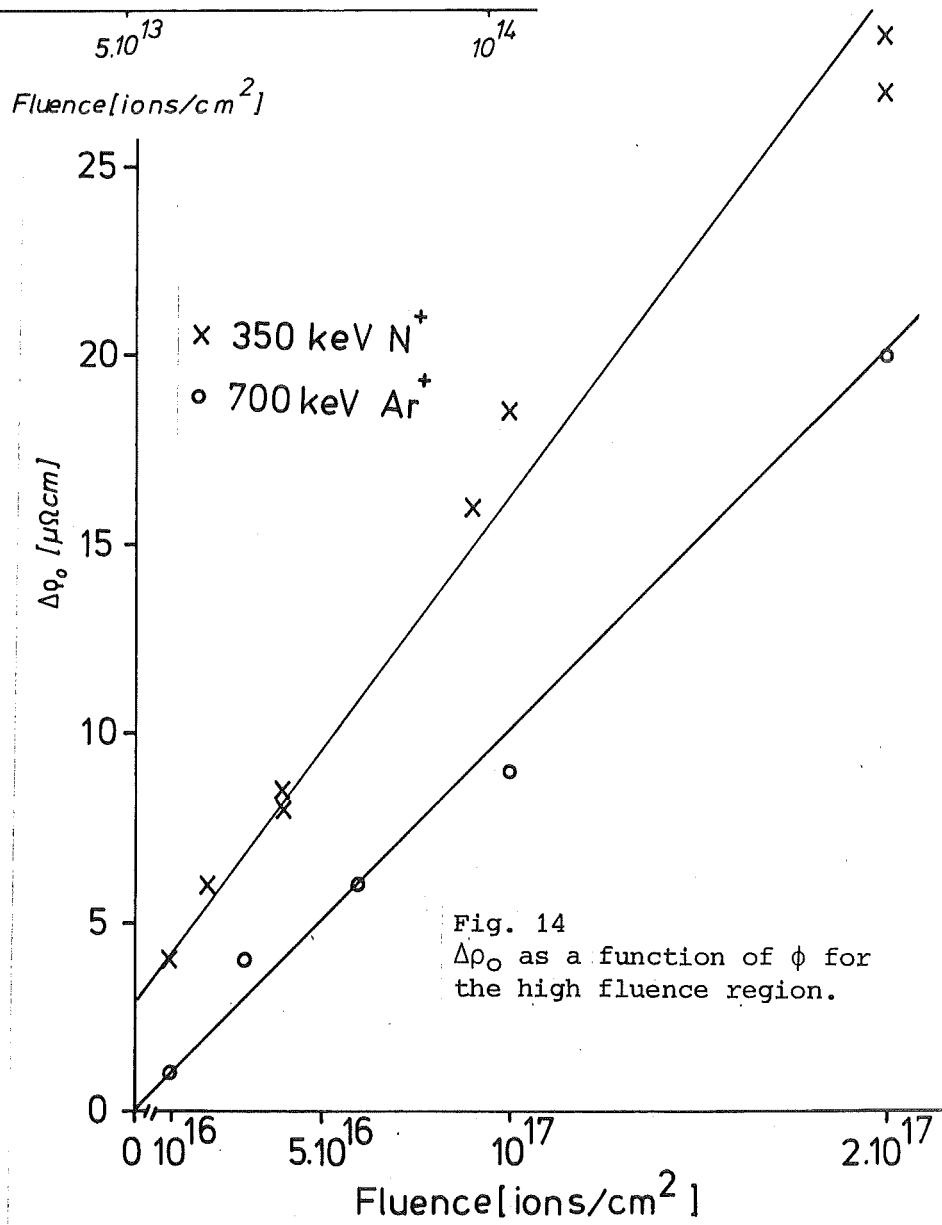the fluence region 10^{12} to
10^{14} ions/cm^2.

x 350 keV N$^+$

o 700 keV Ar$^+$

$\Delta\rho_0$ [$\mu\Omega cm$]

Fluence[ions/cm^2]

x 350 keV N$^+$

o 700 keV Ar$^+$

$\Delta\rho_0$ [$\mu\Omega cm$]

Fig. 14
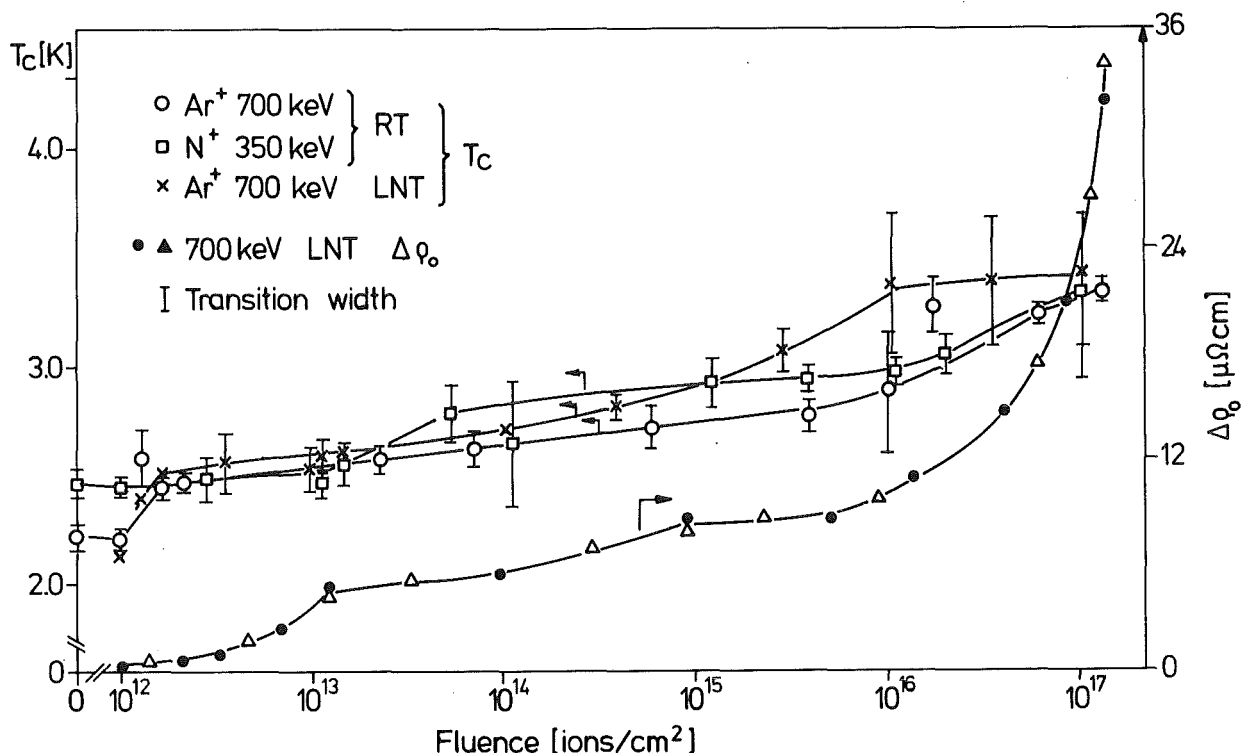$\Delta\rho_0$ as a function of ϕ for
the high fluence region.

Fluence[ions/cm^2]

Fig. 15   The changes in $\Delta\rho_0$ and resistive T_c as a function of Ar-ion · fluence irradiated at LNT. The resistive T_c-values for N- and Ar-irradiations are also plotted.

With increasing ion fluence the ρ_{RT} and ρ_0 were found to increase while ρ_{th} was observed to remain unchanged within the experimental accuracy (18 ± 1 $\mu\Omega$cm) up to 10^{16} Ar-ions/cm^2. Above 10^{16} Ar-ions/cm^2, ρ_{th} decreased. Thus a change in ρ_{th} at high fluences may be due to extended defects.

After each irradiation inductive and resistive T_c-values were measured. The inductive T_c-values as a function of ϕ are also plotted in Fig. 12. Irradiations up to 3 x 10^{13} Ar-ions/cm^2 cause almost no change in inductive T_c whereas for fluences above 3 x 10^{13} Ar-ions/cm^2 a continuous increase up to 2.7 K at a maximum fluence of 2 x 10^{17} Ar-ions/cm^2 is seen. In contrast to this, resistive T_c-values (Fig. 15) indicate a monotonic increase with fluence and saturate above 2 x 10^{16} Ar-ions/cm^2. This different dependence of inductive and resistive T_c on ϕ leads to the following conclusion. The inductive T_c provides information on the volume of superconducting material in the sample and would not be detected by inductive T_c below a critical value whereas the resitive T_c-values require only a small fraction of superconducting material to register a superconducting transition. Thus a high resistive T_c-value as compared to inductive T_c-value indicates an inhomogeneous distribution of the

superconducting material produced in this case by ion irradiations. So the damage production mechanism is inhomogeneous and only a small number of defects are produced which are responsible for T_c-enhancements. This is the reason why resistive T_c increases monotonically in contrast to inductive T_c which remains insensitive at low fluences. Further irradiation increased the volume of these defects which is now indicated by the inductive T_c-values. But the volume of the sample has not completely filled even at high doses. This is predicted by inductive T_c values which shows no saturation at high doses.
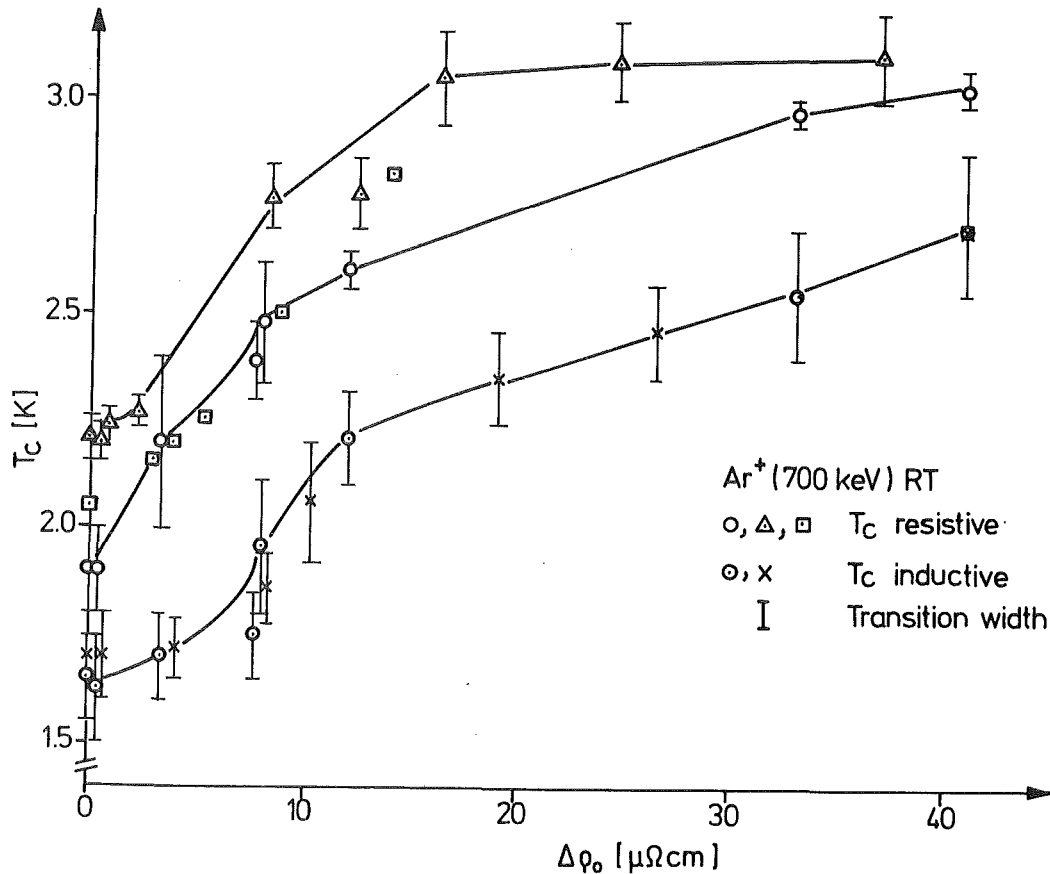

Fig. 16   The changes in resistive and inductive T_c-values as a function of $\Delta\rho_0$ for Ar-ion irradiations.

Figure 15 also shows the resistive T_c-values for a film, irradiated at LNT. As compared to the RT-irradiations no significant difference is registered in this case. The resistive and inductive T_c-values as a function of $\Delta\rho_0$ are plotted in Fig. 16. Inductive T_c-values for two different films as a function of $\Delta\rho_0$ show good agreement and do not depend on the crystalline state or the pre-irradiation ρ_0-values. The post-irradiation resistive T_c-values depend

however, on the pre-irradiation values and different resistive T_c-values belong to the same $\Delta\rho_o$-value. As argued earlier, this may be due to inhomegeneously distributed vacancies pinned to dislocations which have formed at grain boundaries during crystal growth.

3.2.1.2 Structure:

X-ray line intensity measurements were performed before and after each irradiation and the lattice parameter were also determined (Table 8). The cell volume, V_c, was observed to change as a function of Ar-ion fluence. Irradiations with fluences of 10^{12} Ar-ions/cm^2 cause a decrease of 0.7% in cell volume. With increasing Ar-fluence V_c is found to increase by 1.4% and 3% at fluences of 10^{16} and 2×10^{17} Ar-ions/cm^2, respectively.

Table 8

Influence of Ar-ions irradiation at RT on
the lattice parameters and cell volume of Re-films.

Fluence	Lattice parameters		cell volume
[ions/cm^2]	a[Å]	c[Å]	V_c[Å^3]
0	2.764	4.471	29.581
1.10^{12}	2.760	4.454	29.383
4.10^{12}	2.762	4.459	29.459
1.10^{13}	2.764	4.473	29.594
1.10^{14}	2.763	4.509	29.811
1.10^{15}	2.775	4.485	29.910
1.10^{16}	2.778	4.488	29.995
1.10^{17}	2.787	4.500	30.270
2.10^{17}	2.768	4.591	30.469

With increasing fluence, the intensity of almost all lines either decreased or remained unchanged with the exception of the $(10\bar{1}1)$ line where the intensity increased as indicated in Fig. 17. Recrystallisation effects are also registered after irradiation with fluences of 1×10^{14} Ar-ions/cm^2 by channeling measurements. Such an effect has also been noted previously /46/ in neutron irradiated Re-foils.
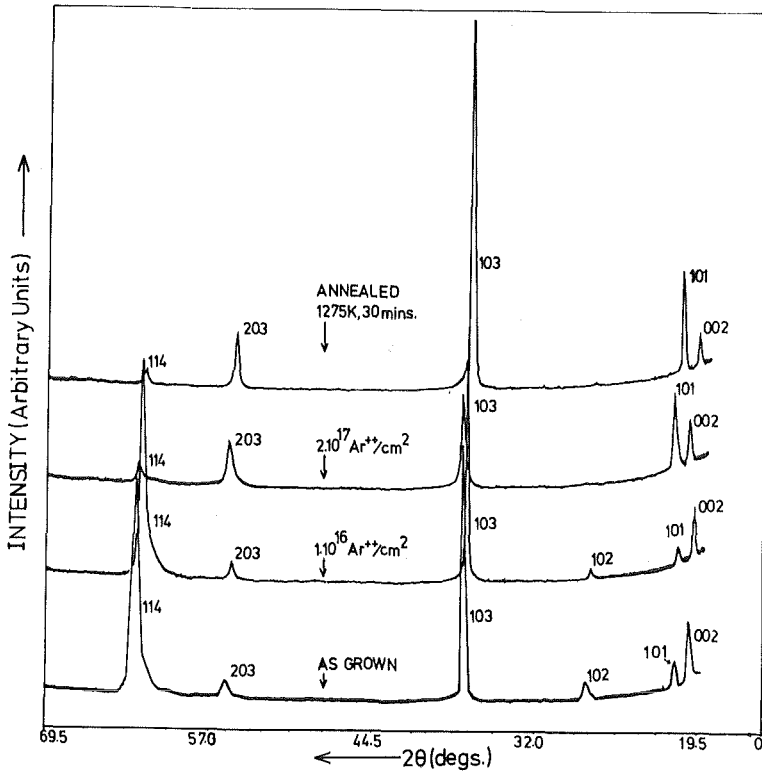
Fig. 17
Diffraction pattern from
Re film before, after Ar-
ions irradiation and annel-
ing at 1275 K.

3.2.1.3 Isochronal Annealing of ρ_o and T_c:

In order to get more information on the nature of ion-induced intrinsic defects poly- and single-crystalline rhenium films irradiated with 2×10^{17} Ar-ions/cm^2 at RT were subjected to isochronal annealing processes. In Fig. 18 the resistive T_c as a function of annealing temperature shows a continuous recovery over the measured annealing temperature. The values of ρ_o and inductive T_c as a function of annealing temperatrue are shown in Fig. 19. In contrast to resistive T_c-values, inductive T_c-values show well resolved recovery curve. Thus it may be concluded that no information about annealing stages can be obtained from resistive T_c-measurements in the case of rhenium. Hence only induc-tive T_c-values are used for the analysis of isochronal annealing curves.

Refering to literature /35/ the recovery curve for ρ_o (Fig. 19) indi-cates three recovery stages from 400 to 600 K (0.11 to 0.17 T_m); 700 to 850 K (0.20 to 0.25 T_m) and 850 to 1200 K (0.25 to 0.35 T_m) for both poly- and sing-le-crystalline films. As will be discussed later, these stages are denoted as stages II, IV and V, respectively /36/. The main differences between the re-covery of poly- and single-crystalline films are seen in stage II which is more pronounced for the single-crystalline film and stage V which is strongest in the case of the polycrystalline film. In both cases complete annealing is not
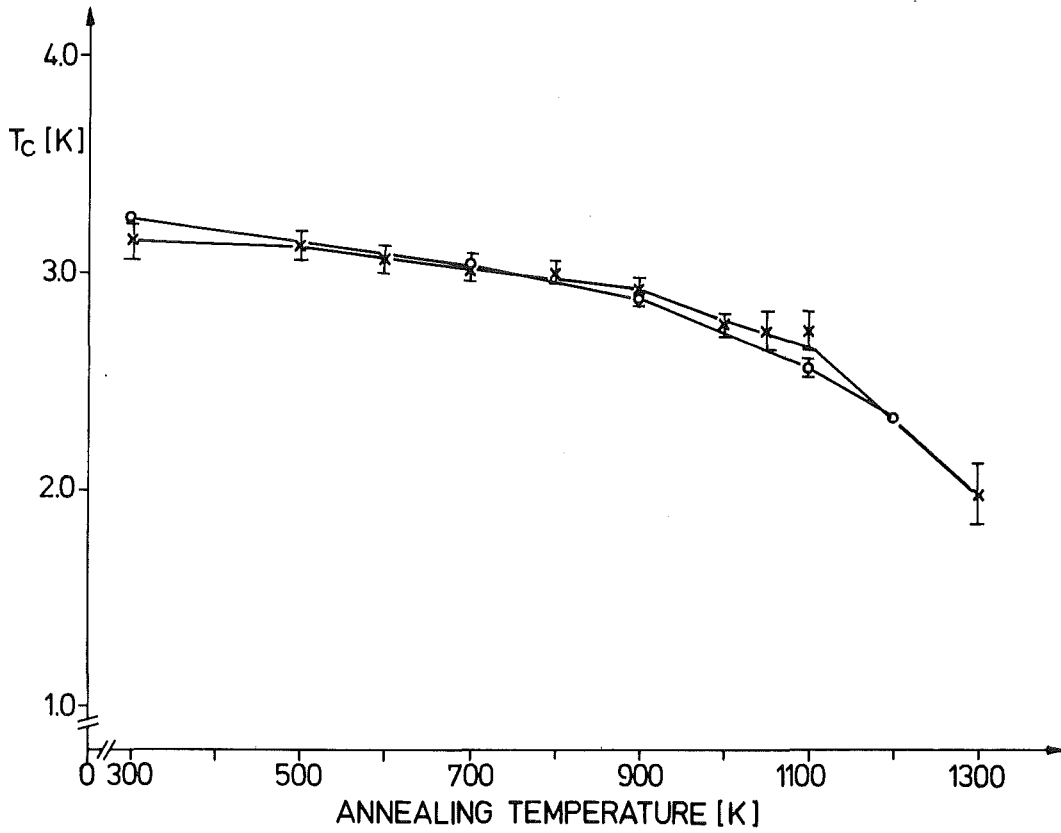
Fig. 18   Resistive T_c-values as a function of annealing temperature irrad-
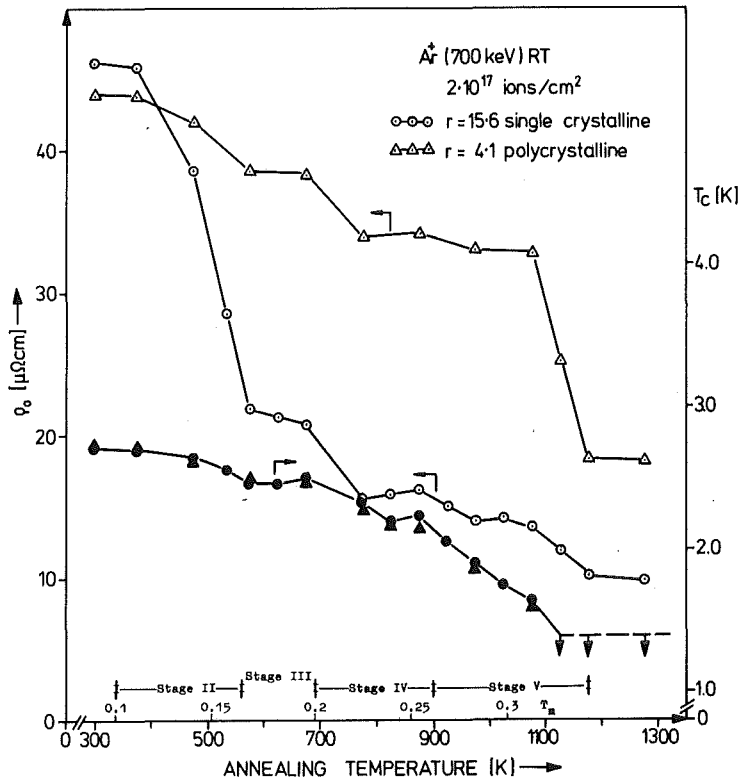iated with 2 x 10^{17} Ar-ions/cm^2.

Fig. 19
Isochronal ρ_0- and
T_c-annealing curves for
poly- and single-crys-
talline films irrad-
iated with
2 x 10^{17} Ar-ions/cm^2.

achieved even at 1275 K. For single-crystalline film about 25% of the radia-
tion induced resistivity is left while for polycrystalline film this frac-
tion is 40%.

The annealing curves for T_c are similar for both single- and poly-
crystalline films. Three recovery stages are also observed for T_c. The maximum
recovery is seen in stage V and complete recovery of T_c is achieved at 1125 K.
It should be pointed out that resistive T_c is not completely annealed even at
1300 K which indicates again that vacancies pinned to dislocations are res-
ponsible for T_c as dislocations still exist in the film.

3.2.2 Influence of N-Ion Irradiation:

Fifteen rhenium films were irradiated with 350 keV N-ions up to a total
fluence of 2×10^{17} ions/cm^2. After each irradiation $\Delta\rho_o$, T_c
and structure were studied with the following results:

3.2.2.1 Ion Induced Residual Resistivity, $\Delta\rho_o$ and T_c:

The increase of $\Delta\rho_o$ with N-ion fluence is shown in Fig. 20. It can be
seen that the values obtained after irradiation of different films show good
agreement. As mentioned earlier, no influence of pre-irradiation properties on
the change in $\Delta\rho_o$ due to irradiation is registered although the as-grown films
had ρ_o-values of 0.9, 1.8, 4.0 and 4.2 $\mu\Omega$cm. Only a small increase of about
0.5 $\mu\Omega$cm in $\Delta\rho_o$ is noted for fluences up to 10^{13} N-ions/cm^2. Above 10^{13}N-ions/cm^2,
$\Delta\rho_o$ increases by 8 $\mu\Omega$cm and shows a saturation between 10^{15} and 7×10^{15}N-ions/cm^2.
For higher fluences $\Delta\rho_o$ increases rapidly and attains a typical value of 29 $\mu\Omega$cm
at 2×10^{17} N-ions/cm^2. Further irradiation caused macroscopic damage of the film.

Similar to the Ar-irradiation results the fluence dependence of $\Delta\rho_o$ seems
to reflect again the production of two different defect structures. The first
type of defect is produced mainly at low fluences (Fig. 13) and saturates at
fluences above 10^{15} N-ions/cm^2. The second type is mainly produced for fluences
(Fig. 14) above 10^{16} N-ions/cm^2. Applying the same analysis procedure as dis-
cussed in section 3.2.1.1, 13 Frenkel pairs are produced per incident N-ion. The
Kinchin and Pease model /42/ predicts 114 Frenkel pairs indicating that only 11%
vacancies survive the stage I annealing. The sharp increase of $\Delta\rho_o$ in the high
fluence region can not be attributed to sputtering or ion beam mixing. In order
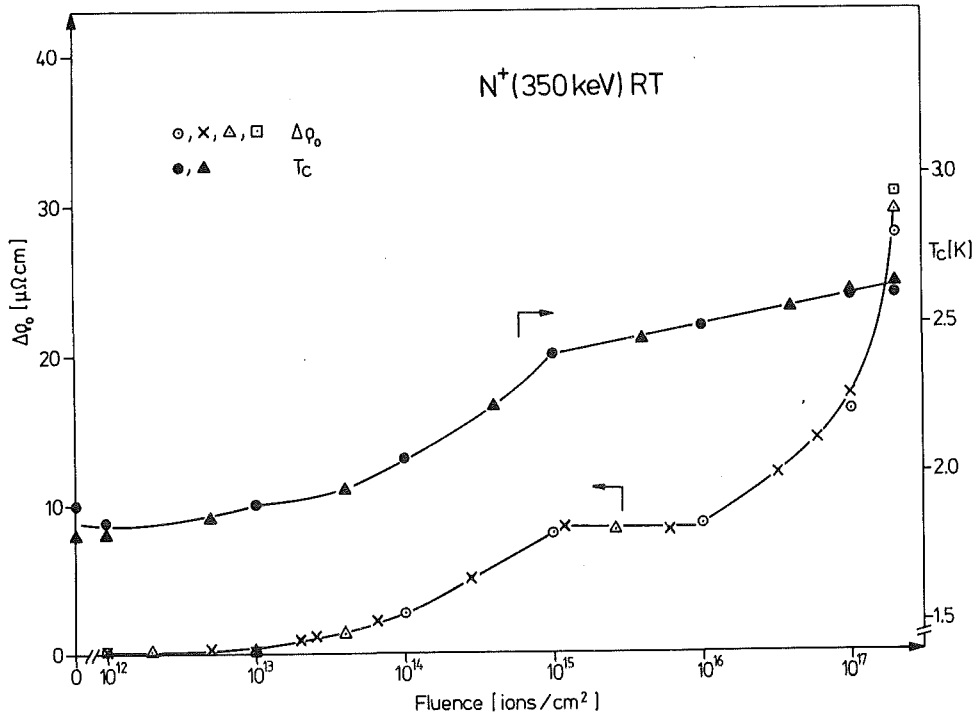
Fig. 20 Changes in $\Delta\rho_0$ and T_c as a function of N-ion fluence. The $\Delta\rho_0$-values for 4 different films and the T_c values for 2 different films with poly- and single-crystalline structures are plotted.

to see if the production of defects in high fluence region does depend on dose rate and temperature, some films were irradiated with fluences of 5×10^{16}; 1×10^{17} and 2×10^{17} N-ions/cm^2 at LNT and RT using three different beam currents of 0.5, 5 and 50 A/cm^2. No remarkable influence on $\Delta\rho_0$ and thus on the production of defects could be seen (Table 9). It is assumed that the large increase of $\Delta\rho_0$ is a result of the formation of extended defects such as dislocations. The production rate of dislocations at high fluences is 1.5×10^{-6} dislocations/ion.

After each irradiation besides $\Delta\rho_0$, inductive and resistive T_c-values were also measured. The inductive T_c-values as a function of fluence are also plotted in Fig. 20. These values for different films show good agreement. The increase in inductive T_c as a function of ion fluence is additive with respect to the pre-irradiation inductive T_c-values. In the fluence region up to 10^{13} N-ions/cm^2, the increase is small. Above this fluence T_c increased from 1.9 K to 2.4 K with increasing fluence up to 10^{16} N-ions/cm^2 and nearly attains a saturation value of 2.64 K at the maximum fluence of 2×10^{17} N-ions/cm^2. In this case also resistive T_c-values show the same dependence on fluence as for Ar-irradiations (Fig. 15) except that resisitve T_c-values do not seem to saturate at high fluences.

The comparison of Fig. 12 and 20 indicates that the inductive T_c-values increased more strongly for N-irradiations as compared to Ar-irradiations. This could be due to the following reasons: The low inductive T_c-values in the case of the Ar-irradiation were attributed to the inhomogeneous distribution of vacancies. While for N-irradiations, the defect-impurity complex may be formed with the N-ions which came to rest in the Re-films and this could be responsible for the high inductive T_c-values. To confirm this hypothesis, two Re-films of thicknesses 600 Å were irradiated with 350 keV Ne- and 700 keV N-ions at RT. Increase in $\Delta\rho_o$ and inductive T_c were compared at the same Q-values with 350 keV N- and 700 keV Ar-irradiations. No difference in $\Delta\rho_o$-values was observed. Inductive T_c-values for Ne- and Ar-ions were of the same order. T_c-values for 700 keV N-ions were larger as compared to Ne- and Ar-ions but were smaller than the 350 keV N-ion values. Calculations have shown that in case of 700 keV N-ions about 10% ions i.e. 0.1% At N came to rest at the interface of the film as compared to the 350 keV N-ions which were 0.5% At. Thus high inductive T_c-values for N-irradiations are a result of defects stabilized by these ions. Extra care should be taken, if irradiation experiments are to be performed with the chemically active ions.

Table 9

Influence of dose rate and temperature on $\Delta\rho_o$ and T_c-values

Fluences	5×10^{16} N-ions/cm^2			1×10^{17} N-ions/cm^2			2×10^{17} N-ions/cm^2			Temp.
beam current [μA]	0.5	5	50	0.5	5.	50	0.5	5	50	
$\Delta\rho_o$ [μΩcm]	13.0	12.6	15.5	18.6	18.2	18.5	26.4	26.8	27	RT
resistive T_c[K]	2.24	2.80	2.67	2.85	2.90	2.87	2.9	2.9	3.1	
inductive T_c [K]	2.50	2.45	2.52	2.55	2.50	2.53	2.6	2.58	2.65	
$\Delta\rho_o$ [μΩcm]	12.4	12.8	16.0	18.0	18.5	18.2	27.0	27.4	27.6	LNT
resistive T_c[K]	2.30	2.50	2.45	2.75	2.95	2.88	2.95	3.1	3.0	
inductive T_c[K]	2.45	2.40	2.43	2.60	2.52	2.55	2.65	2.60	2.68	

3.2.2.2 Structure:

X-ray line intensity and lattice parameters were also determined after each irradiation. The cell volume, V_c (Table 10) was observed to change as a function of N-ion fluence. Irradiations with fluences of 10^{12} N-ions/cm^2 caused a V_c decrease of 0.15%. Irradiations with 3×10^{12} N-ions/cm^2 caused a slight increase in V_c of about 0.1%. Further irradiations up to 10^{13} N-ions/cm^2 caused no change in V_c. Above 10^{15} N-ions/cm^2, V_c becomes 0.4% larger as compared to the pre-irradiation value. Additional irradiations caused a further increase in cell volume and at 2×10^{17} N-ions/cm^2 V_c was 3.4% larger than for a non-irradiated film.

With increasing fluence, the intensity of almost all lines, either decreased or remain unchanged with the exception of the $(10\bar{1}0)$ line whose intensity increased (Fig. 21). At maximum fluence all lines nearly disappeared with the exception of $(10\bar{1}0)$, $(10\bar{1}1)$ and $(10\bar{1}2)$. This result indicates an ion induced recrystallization effect in the $(10\bar{1}0)$ direction (Fig.21).The effect is most pronounced in nearly single-crystalline films and was confirmed by channeling measurements using 2 MeV He-particles. Such an effect has also been noted previously /46/ in neutron irradiated Re-foils.

Table 10

Influence of N-ions irradiations on the lattice
parameters and cell volume of Re-films.

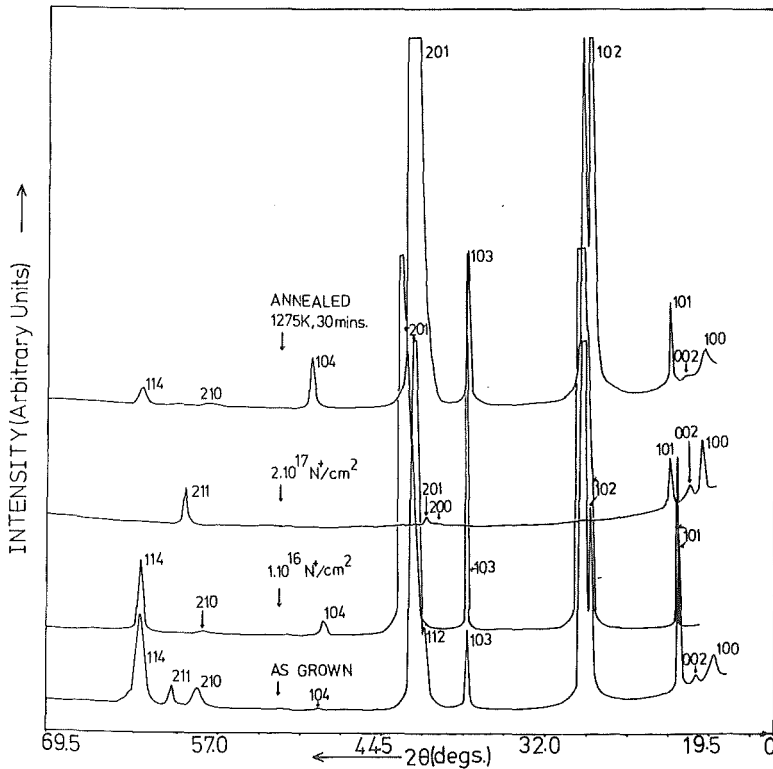| Fluence	Lattice parameters		cell volume
[ions/cm^2]	a [Å]	c [Å]	[Å^3]
0	2.762	4.459	29.459
1.10^{12}	2.761	4.456	29.417
3.10^{12}	2.762	4.457	29.446
1.10^{13}	2.763	4.54	29.447
1.10^{14}	2.763	4.462	29.500
1.10^{15}	2.767	4.461	29.579
1.10^{16}	2.775	4.500	30.010
1.10^{17}	2.773	4.553	30.320
2.10^{17}	2.780	4.551	30.460

Fig. 21
Diffraction pattern from
Re-film before and after
N -ion irradiation and
annealing at 1275 K.

3.2.2.3 Isochronal Annealing of ρ_O and T_c:

Isochronal annealing processes have been applied to poly- and single-crystalline Re-films irradiated with 2 x 10^{15} N-ions/cm^2 and 2 x 10^{17}N-ions/cm^2. The recovery of both ρ_O and inductive T_c for films irradiated to high and low fluences is shown in Fig. 22. For films irradiated at high fluence three main recovery stages are noted which are located between 400 and 600 K (0.10 to 0.17 T_m), 700 and 900 K (0.20 to 0.26 T_m) and 925 to 1200 K (0.27 to 0.35 T_m) (T_m = melting point of Re). Stages II and V are most pronounced for the ρ_O recovery of both poly-,as well as,single-crystalline films and about 8% and 4% radiation induced residual resistivity is left,respectively,even at 1275 K. The recovery of T_c also shows three recovery stages in the same temperature regions which are nearly equal in magnitude (Fig. 22).
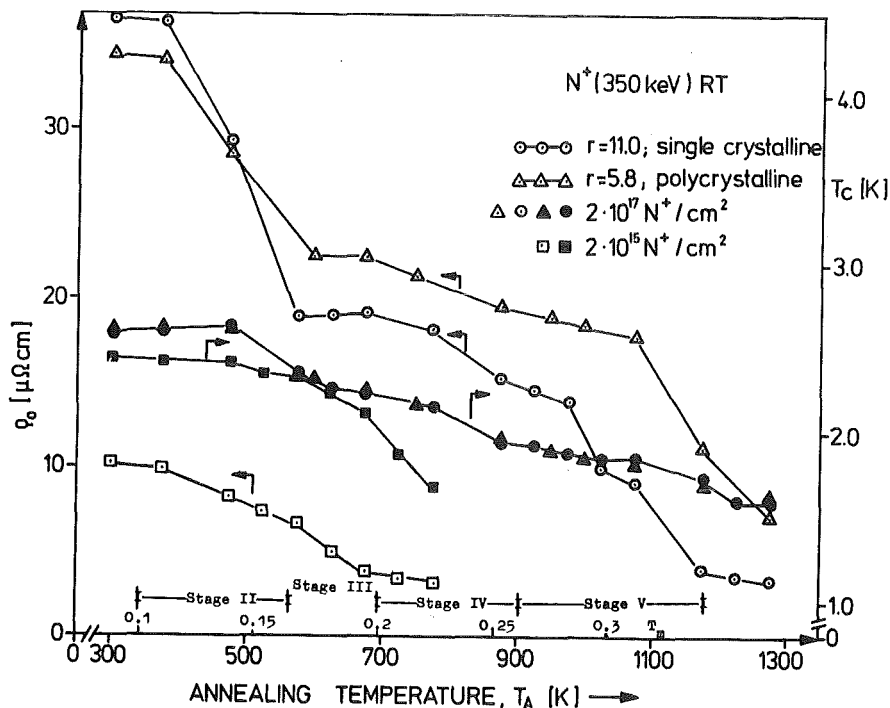

Fig. 22 Isochronal ρ_O- and T_c-annealing curves for poly- and single-crystalline films irradiated with 2 x 10^{17} N-ions/cm^2. The annealing curve for a film irradiated with 2 x 10^{15} N-ions/cm^2 is also plotted for comparison.

The low dose irradiated film shows just one recovery stage having a shoulder for ρ_o between 400 and 700 K (0.12 to 0.20 T_m) and for T_c between 550 and 800 K (0.16 to 0.23 T_m). This shift in annealing temperature between $\Delta\rho_o$- and T_c-recovery is unusual and will be discussed below. The observed recovery of $\Delta\rho_o$ at 0.17 T_m as noted after neutron irradiation is attributed to stage III /35/.

3.3 Ion Implanted Metastable Phases:

In order to produce impurity-stabilized defects and metastable phases, homogeneous ion implantation (also called ion implantation) experiments were performed. The energies of the ions and their fluences required for homogeneous ion implantation were calculated as described in section 2.2. Argon as an inert gas has been implanted to produce possible mechanical effects e.g. development of high stresses in the film and to study their influences on the resistivity, T_c and structure of the Re-films. N- and P-ions have been implanted as chemically active impurities to obtain impurity stabilized defects or metastable phases and to separate their influence on structure, resistivity and T_c of the Re-thin films.

3.3.1 Homogeneous Implantation of Ar-Ions:

The Ar-ions were homogeneously implanted in two Re-films at RT. The films had poly- and single-crystalline structure with r-values of 3 and 15, respectively. The changes in resistivity and inductive T_c as a function of Ar-ion implantations is presented in Fig. 23. A rapid increase in ρ_{RT} is registered for low Ar-concentrations up to 1 at% Ar. Between 1 and 20 at% Ar a linear increase in ρ_{RT} is observed which seems to saturate above 20 at% Ar and attains a saturation value of 72 $\mu\Omega$cm. No implantations above 26 at% Ar could be performed as the films were macroscopically damaged. The ρ_{RT}-value at 6 at% is comparable with the ρ_{RT}-value of 57 $\mu\Omega$cm, obtained due to intrinsic defects produced by irradiation with 2×10^{17} Ar-ions/cm^2. Thus an additional increase of about 15 $\mu\Omega$cm in ρ_{RT} is registered due to Ar-ion implantation. This could be due to sputtering, ion beam mixing with the substrate, high stress values or blistering. The values of ρ_{RT} plotted in Fig. 23 have already been corrected for sputtering effect. Ion beam mixing was not observed by RBS measurements.
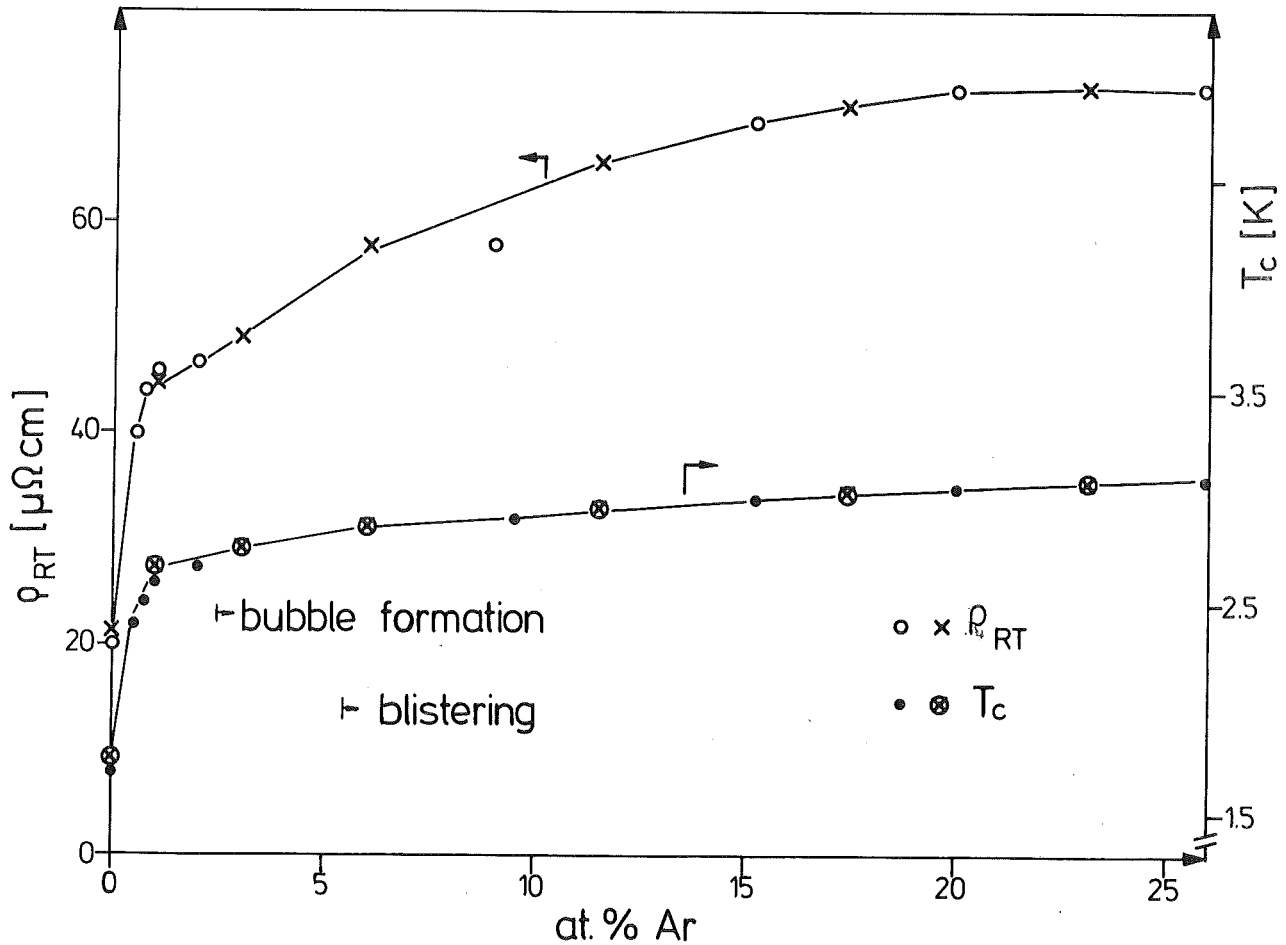
Fig. 23 ρ_{RT}- and inductive T_c-values as a function of Ar-ion concentration, implanted at RT.

The stress value as a function of Ar at% was calculated according to the method described in section 2.5. The stress value increased up to 1 at% Ar. At this stage it was 8×10^{10} dynes/cm^2 as compared to the pre-implantation value of 0.3×10^{10} dynes/cm^2. Above 1 at% Ar-stress was observed to decrease as a function of Ar-concentration. Thus stress cannot be responsible for increases in the ρ_{RT}-value. To check if bubble formation and blistering takes place, the Re-films with Ar-concentrations of 1,2,3,5,6,8,12 and 20 at% were investigated in a scanning electron microscope. The electron micrographs are shown in Figs. 24 and 25. Bubble formation is observed above 2 at% and blistering started above 5 at%.Figure 25 shows the blistering after implantation of 8 at% Ar. Making the assumption that the holes observed in the film due to blistering go through the film thickness, their area of cross section was measured. This area was substracted from the area used to calculate the resistivity. These

├───┤ 7.14 µ
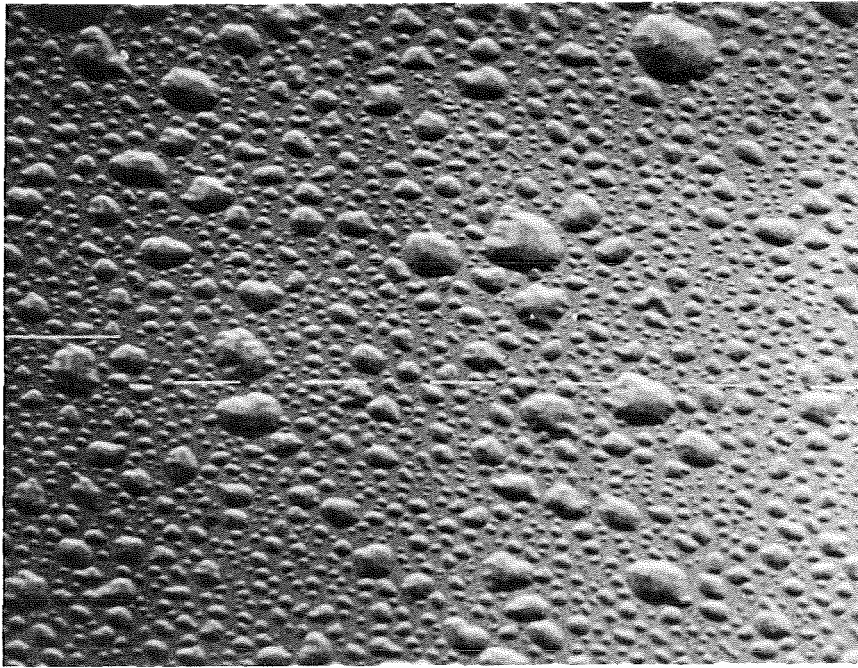
Fig. 24   Bubble formation shown by electron micrograph of Re-film
implanted with 3 at% Ar, at RT.

├──┤ 7.14 µ
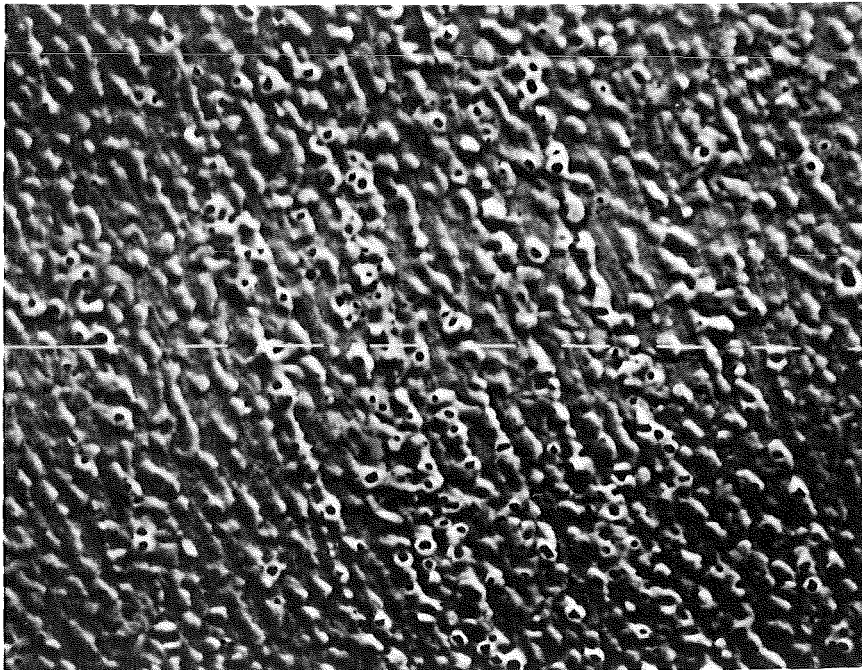
Fig. 25   Blistering indicated by electron micrograph of Re-film
implanted with 8 at% Ar at RT.

measurements indicated that at 8 at% Ar, the decrease in areal cross section
was about 10% i.e. the value of ρ_{RT} measured here should be about 10%
smaller. Thus it is concluded that the larger ρ_{RT}-value for implantation as
compared to irradiation is due to blistering and not to an increase in
damage density and mechanical defects do not seem to influence the ρ_{RT}.

    As shown in Fig. 23, the inductive T_c-values increase as a funciton
of Ar-concentrations. At 6 at% Ar, a T_c-value of 2.85 K is registered. The
same T_c-value was obtained due to the influence of intrinsic defects at the
maximum fluence used. Implantations up to 26 at% Ar caused a further increase
of 0.25 K. The resistive T_c also increased as a function of Ar-concentra-
tion and a value of 3.6 K was recorded at 26 at% Ar. Somewhat larger in-
ductive T_c may be a result of the fact that during Ar-irradiation no satura-
tion was observed.

3.3.2 Rhenium Nitride Phases:

    The solubility of N in Re is very small at room temperature /33/. Seven
Re films were implanted with N-ions at 475 K, RT and LNT. The films had poly-
or single-crystalline structures and r-values between 5 and 15. No influence
of the crystalline state of pre-implanted films on the resistivity and T_c of
the implanted films was observed.

3.3.2.1 Structure of N-Implanted Re-Films with the Implantation Temperature as a Parameter:

    To study the structural changes in the polycrystalline Re films, N-ions
up to 50 at% were homogeneously implanted at RT. For this purpose no single-
crystalline film was used as thin film X-ray diffraction method was not able
to provide information about structural changes in these films. The cell vo-
lume, V_c, of the hcp Re changed from 29.487 $\overset{\circ}{A}^3$ to 30.313 $\overset{\circ}{A}^3$ as a result of
N-implantations up to 6 at%. Between 6 and 12 at% N, a new metastable phase
was observed in adddition to the hcp Re-structure. The d-values of this phase,
at 9 at% N are given in Table 11 column 1. Structure of this phase which is

Table 11

d-values and intensities, I, for $ReN_{0.09}$, $ReN_{0.31}$, $ReN_{0.45}$ and ReN

9 at% N = Re N$_{0.09}$		31 at% N = ReN$_{0.31}$				45 at% N = ReN$_{0.45}$				50 at% N = ReN			
d-value [Å]	I	d-value [Å]	h k l		I	d-value [Å]	h k l		I	d-value [Å]	h k l		I
2.322	s	2.307	1 1 1		s	2.311	1 1 1		s	2.321	1 1 1		s
1.403	s	1.998	2 0 0		m	2.002	2 0 0		m	2.010	2 0 0		m
1.067	m	1.417	2 2 0		m	1.415	2 2 0		m	1.422	2 2 0		m
0.943	m	1.209	3 1 1		s	1.208	3 1 1		s	1.212	3 1 1		s
0.850	w	1.157	2 2 2		vw	0.919	3 3 1		w	1.160	2 2 2		vw
		0.920	3 3 1		w	0.896	4 2 0		w	0.922	3 3 1		w
		0.897	4 2 0		w					0.899	4 2 0		w
		0.819	4 2 2		w					0.820	4 2 2		w
		a = 4.003 ± 0.003				a = 4.006 ± 0.008				a = 4.021 ± 0.002			

s = strong; m = medium; w = weak; vw = very weak.

denoted by $ReN_{0.09}$ could not be identified. At N-concentrations above 12 and up to 45 at% besides hcp Re and $ReN_{0.09}$, an additional phase was detected. This phase has a fcc(B1) structure and its lattice parameter increased with the increase in N at%. Lattice parameter and d-values for this phase at 31 and 45 at% N are shown in Table 11 column 2 and 3, respectively. Above 45 at% only fcc phase was observed. The lattice parameter of this phase at 50 at% N is 4.021 ± 0.002 Å. The d-values of this phase are also presented in column 4 of Table 11. The lattice parameter of fcc phase has been observed to change from 3.93 to 4.02 Å as the N-concentration in the film varied from 13 to 50 at%. The ReN phase formed at 50 at% N has very sharp lines, and most probably has a NaCl structure with a lattice parameter of 4.021 Å. The existance of this phase was predicted by computer calculations /33/.

In Fig. 26, the changes in the stress value as a function of N-concentration are plotted. Unexpectedly high stresses of about 14×10^{10} (at 9 at% N) and 98×10^{10} (at 45 at% N), dynes/cm^2 were recorded as compared to the pre-implantaiton stress value of 3×10^9 dynes/cm^2. However, at 31 at% a small increase of 4×10^{10} dynes/cm^2 is also noted. As described earlier, at the same concentrations X-ray lines of the new metastable phases (Table 11) are observed.
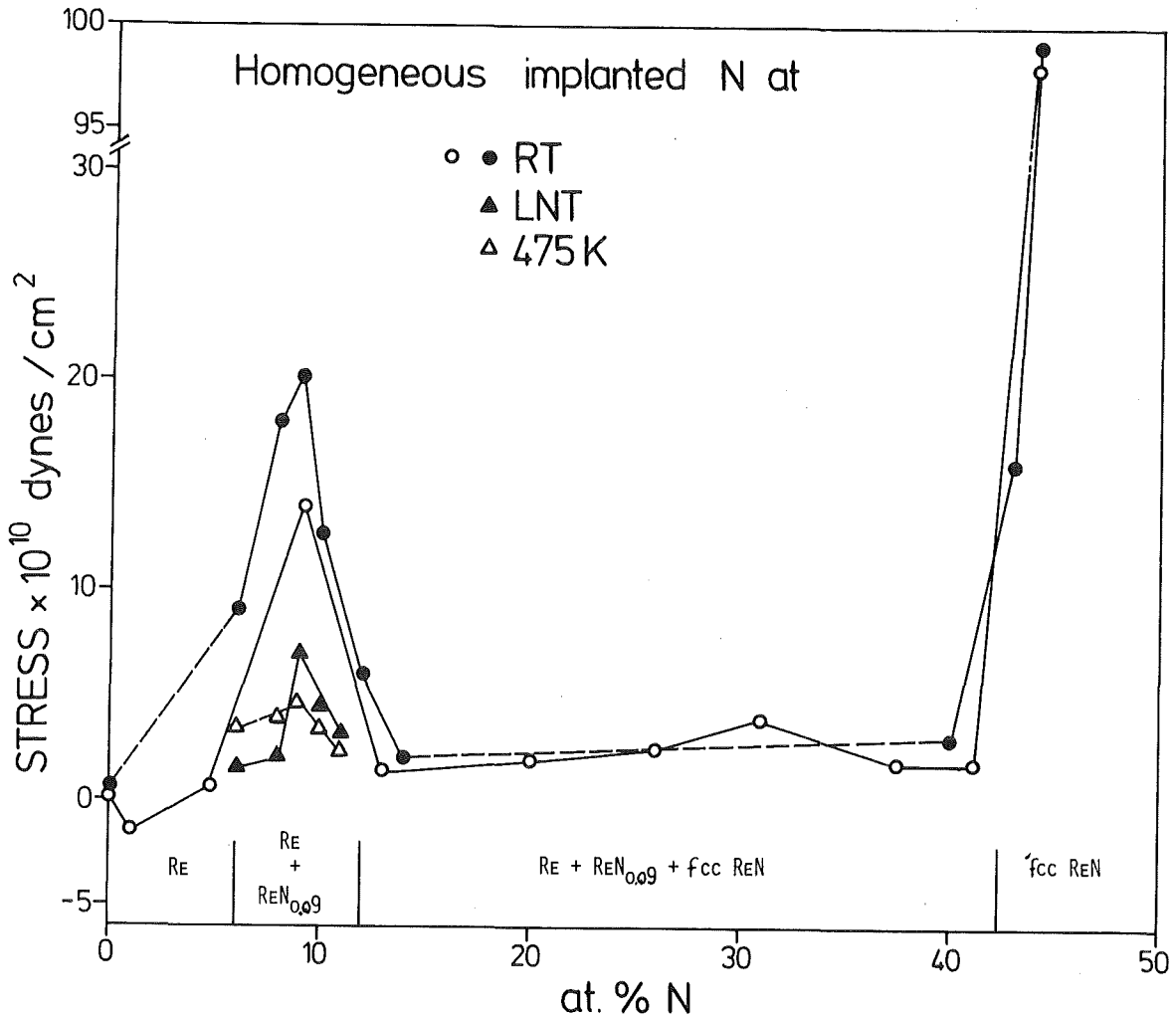
Fig. 26 Stress as a function of N-ion concentration, implanted at 475 K, RT and LNT.

The influence of substrate temperature during implantation on the formation of the above mentioned phases is also investigated. The implantations at 475 K could not be performed above 12 at% N as films were macroscopically damaged probably due to N-bubble formation and blistering. However, at 9 at% N the $ReN_{0.09}$ was observed. Its d-values were comparable with Table 11 column 1. A rather small increase in stress (Fig. 26) is also observed as compared to the RT implanted sample. This small stress value probably results from the fact that implanted N is utilized in bubble formation and later in blistering.

The LNT implantation caused the same structural changes as observed in case of the RT implantations except that above 42 at% N, all X-ray lines disappeared. This phase may either be rhenium nitride with very small crystallites or amorphous rhenium.

3.3.2.2 Resistivity and T_c of Rhenium Nitride Phases:

The RT-resistivity of the homogeneously implanted Re-films with N at RT, LNT and 475 K are plotted in Fig. 27. The ρ_{RT}-values for three films are given as a function of N-concentration for ρ_{RT} implantation. Two films show good agreement while the third film has somewhat higher ρ_{RT}-values for the same N-concentration. The reasons for this discrepancy are not clear. An error in the estimation of implanted N-concentrations may be a possible explanation. Resistivity at RT, ρ_{RT} increases with N-concentration and attains a value of about 180 $\mu\Omega$cm at 41 at% N. At 43 at% N, this value increased to 250 $\mu\Omega$cm and then decreased to 50 at% N, where its value is 230 $\mu\Omega$cm. This decrease in resistance may be due to the formation of an ordered structure such as ReN, which is indicated by X-ray results.
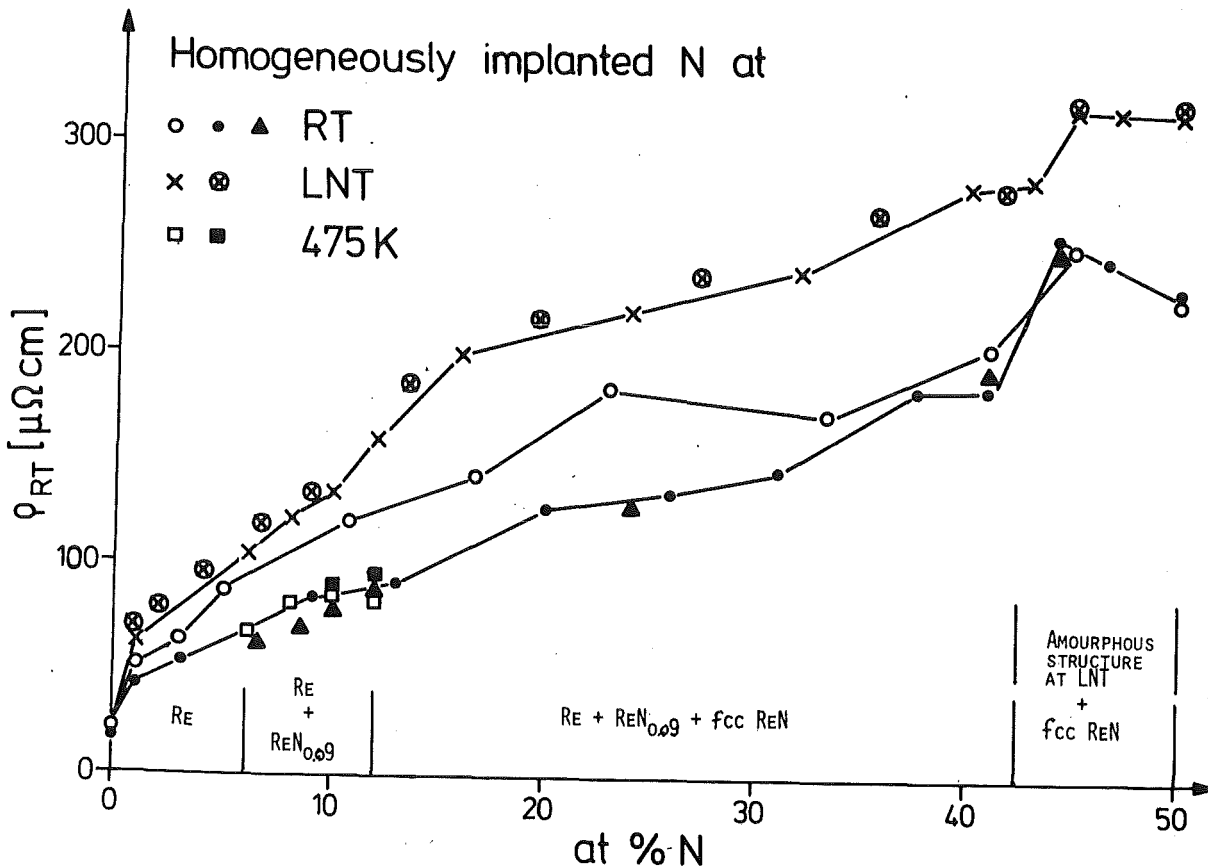

Fig. 27 Increase in ρ_{RT} due to homogeneous ion implantations of N at 475 K, RT and LNT.

The N-implantations at LNT also showed the increase in ρ_{RT} as a function of N-concentration. However, in this case, values of ρ_{RT} were higher when compared to the RT implantations. Here also an increase in resistivity was registered at 43 at% N but then it remains unchanged up to 50 at% N with a value of 320 $\mu\Omega$cm. This resistivity value may be attributed either to microcrystalline rhenium nitride or amorphous Re. The increase in ρ_{RT} values as a function of N-concentration at 475 K were the same as observed for RT-implantations.
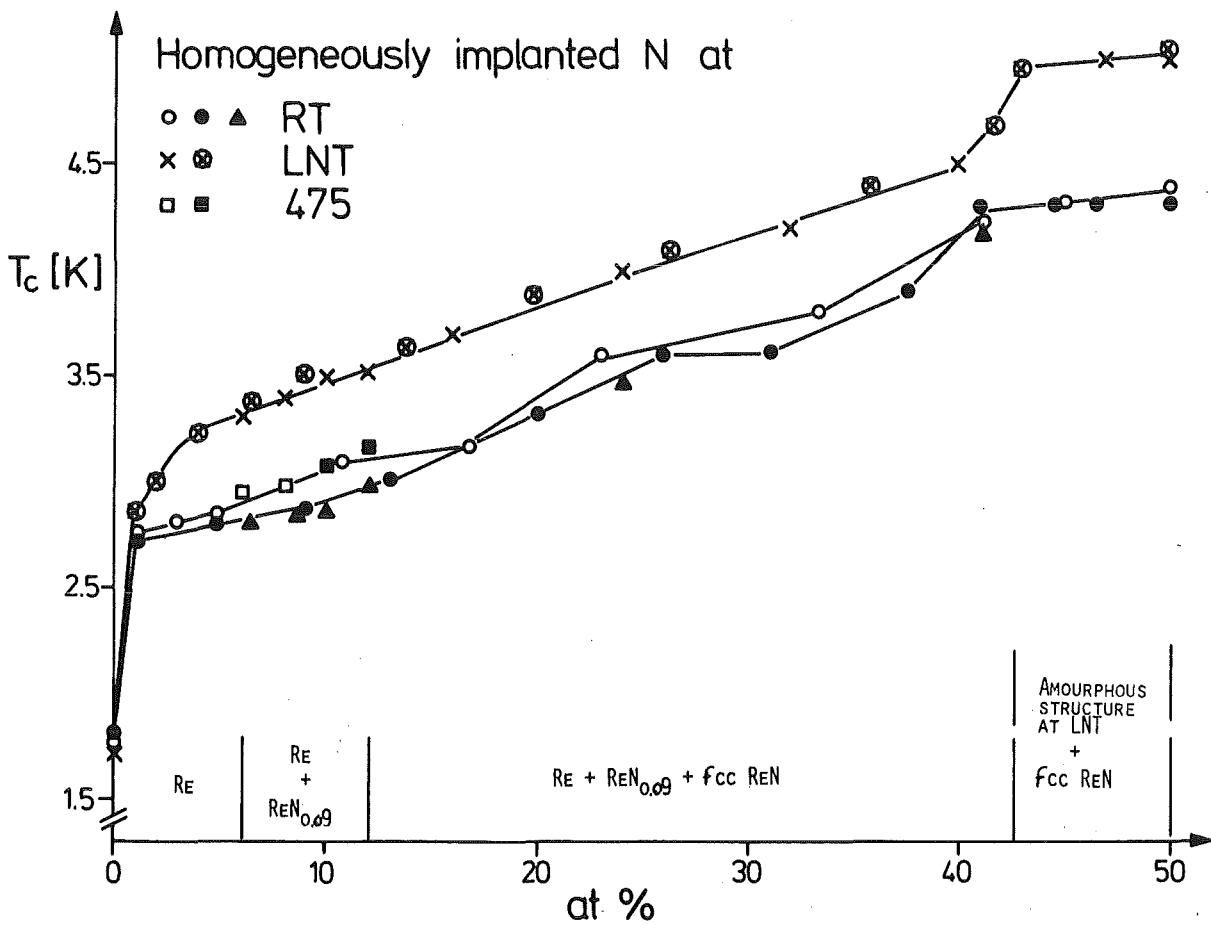

Fig. 28 Increase in inductive T_c as a function of N-ion implantation at 475 K, RT and LNT.

The inductive T_c-values as a function of N-concentration implanted at RT, LNT and 475 K, are plotted in Fig. 28. The implantations of 1 at% N at all the three implantation temperatures caused a rapid increase in inductive T_c up to a value of 2.7 K. The same T_c-value was observed after the irradiation by 2×10^{17} N-ions/cm^2. The T_c-values are found to increase as a function of N-concentration.

The inductive T_c-values of 6 and 9 at% N are 2.9 K and 3.1 K, respectively. The T_c-value of 2.9 K may be attributed to the defects stabilized by N-atoms, as is discussed below, whereas T_c-value of 3.1 K may be attributed to either N-defects complexes or to $ReN_{0.09}$. Above 40 at% N, T_c-values seem to saturate. At this stage inductive and resistive T_c-values were 4.0 K and 4.5 K, respectively, which may be attributed to the ReN phase. The N-implantations at 475 K up to 12 at% caused the same increase in inductive T_c as observed after RT-implantations.

The LNT implantations as a function of N-concentration caused higher T_c-enhancements as compared to RT-implantations. T_c-values at 6 and 9 at% N were 3.3 K and 3.5 K, respectively, while resistive T_c-values were 3.6 K and 4.0 K. Further implantation caused a linear increase in T_c. The T_c-value between 45 to 50 at% N was 5 K. Where a resistive T_c-value of 6 K was registered. This could result from either microcrystalline ReN or amorphous Re-phase stabilized by N-atoms.

3.3.2.3 Annealing Experiments:

It is interesting to note that Re-films implanted with 50 at% N at RT and LNT and stored at RT for two months showed annealing effects. The RT implanted films showed an increase in ρ_{RT}-values from 230 ± 5 μΩcm to 270 ± 8 μΩcm and a decrease in inductive T_c-values from 4.0 ± 0.1 K to 3.5 ± 0.2 K. In contrast, LNT implanted films showed no change in ρ_{RT}-values while T_c-values decreased from 5.0 ± 0.1 K to 4.2 ± 0.2 K as a result of storage. The films were isochronically annealed up to 775 K. These results are presented in Fig. 29.

Initial annealing of the film, which was implanted at RT, showed a slight increase in the ρ_{RT}-values up to 375 K. Further annealing showed some variations in ρ_{RT} up to 615 K and then a decrease to 100 μΩcm at 715 K. Inductive T_c values showed some fluctuations as a function of annealing temperature and an increase in T_c was observed near 615 K corresponding to a T_c-value of 4.0 K. Above 645 K a rapid decrease in T_c-values was observed and at 715 K a T_c-value of 1.9 K was obtained. X-ray studies have shown three phases namely Re, $ReN_{0.09}$ and ReN between 350 and 600 K in these films. Above 680 K only hcp Re phase was observed. Thus increase in T_c and decrease in ρ_{RT} at 645 K may result from an improvement in the ordering of the ReN which, however, decomposed above 645 K. The above mentioned effect may also be attributed to the ordering of
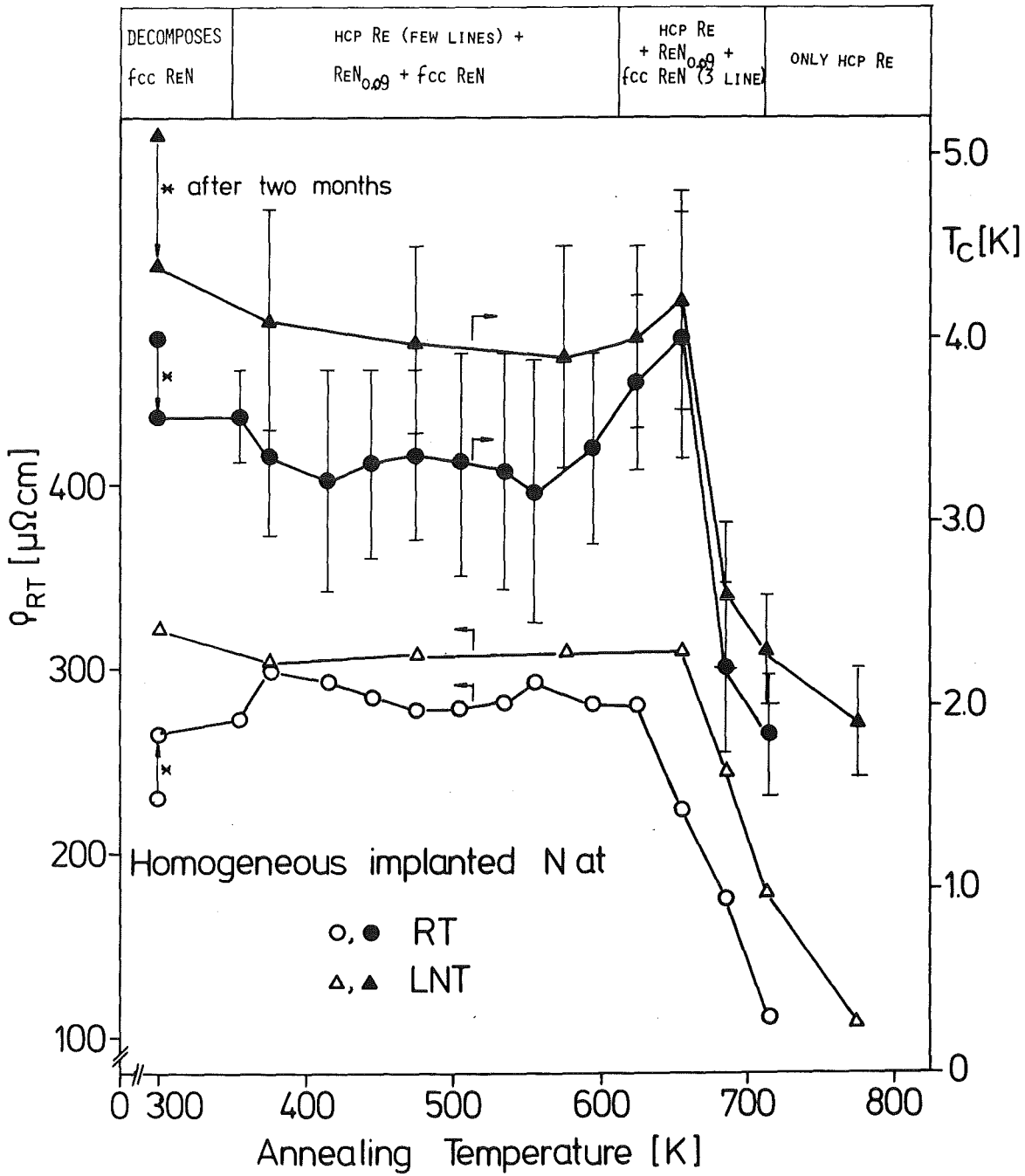
Fig. 29 Changes in ρ_{RT} and inductive T_c as a function of annealing temperature.

$ReN_{0.09}$. To check, this, a film with only Re and $ReN_{0.09}$ structures was annealed. No improvement in T_c or ρ_{RT} was registered. Thus it was confirmed that the high value of T_c at 645 K results from the ReN phase.

The annealing results of the film implanted at LNT are also presented in Fig. 29. The ρ_{RT}-value for this film remained constant up to 645 K and then

decreased rapidly to a value of 100 $\mu\Omega$cm at 775 K. Inductive T_c values showed some variations between 300 and 600 K and increased to a T_c-value of 4.2 K near 645 K. As has been mentioned earlier, this film showed no X-ray line after implantation of 42 at% N at LNT. Two months storage of this film at RT showed two diffuse Re-lines. With the increase in annealing temperature the number of X-ray lines increased and at 645 K, seven x-ray lines were observed. Four of them come from hcp Re, two from ReN and one line from $ReN_{0.09}$. However, at that level of investigation it was difficult to decide if the T_c value of 4.2 K observed at 645 K resulted from microcrystalline ReN or amorphous Re.

3.4 Amorphous Re-Phase:

Phosphorus is a well known glass forming agent. In Re-P systems four rhenium phosphides are known /47/ which are not superconductors /48/. Assuming that microcrystalline rhenium phosphides are also normal conductors, it was expected that P-ion implantations would be helpful in deciding if the high T_c-values of 6 K resulted from microcrystalline rhenium nitride or amorphous Re.

The P-ions were homogeneously implanted at LNT in two Re films of thicknesses 500 Å and 550 Å. At 20 at% P an amorphous structure is observed. Both, the inductive and resistive T_c-values were 6 K and ρ_{RT}-values were 250 to 300 $\mu\Omega$cm. High sputtering effects were seen and the film thickness reduced to 250 Å after implantation of 20 at% P. Since the mean free path of conduction electrons in Re is somewhat larger than 250 Å, (the film thickness obtained after implantation) there is some doubt about the values of T_c and ρ_{RT}. Therefore two Re-films of 3000 and 4500 Å were implanted with 20 at% P over a depth of 1500 Å. X-ray studies again indicated an amorphous structure without additional X-ray lines of any of the rhenium phosphides. Here inductive T_c-values of 6.6 to 6.9 K were obtained with resistive T_c-values of 6.9 to 7.0 K. Thus the amorphous phase of Re has a T_c-value of 6.9 K (resistive T_c-value 7.0 K) and resistivity values between 250 and 300 $\mu\Omega$cm. Isochronal annealing experiments indicated that this phase was stable up to 900 K. So it can be concluded that stability of the amorphous phase depends on the glass former because decomposition temperature for the N-stabilized amorphous phase is 645 K which is smaller than for the P-stabilized amorphous phase.

4. Discusion and Conclusions:

4.1 Properties of Re-Thin Films:

The films grown on polished substrates at $T_s \leq 900$ K always showed a poly-crystalline structure whereas the films grown above 1100 K were always single-crystalline. This is in agreement with the work of Komashko et al. /47/, who also observed the growth of single-crystalline films at high substrate tempe-ratures. The single-crystalline films have ρ_{RT}-and T_c-values comparable to those of the bulk material. Within the experimental accuracy of the present work, the Matthiessen rule is valid for these films (Fig. 6).

At lower substrate temperatures, high values of ρ_o and T_c are observed and the Matthiessen rule is no longer valid. It was shown that these enhanced values of ρ_o and T_c are caused neither by impurities nor by elastic strains but are resulted from defects. Since the average grain size changes only weakly with the substrate temperature and different ρ_o-values are obtained for films grown on polished and rough substrates at a constant value of grain size it is con-cluded that grain boundaries do not contribute strongly to the resistivity of the films.

Annealing experiments of the films grown at low substrate temperatures indicate a large decrease of T_c (Fig. 8) between 600 K (0.17 T_m) and 1000 K (0.32 T_m). A similar decrease in ρ_o and T_c in the same temperature region is observed during film growth (Figs. 6 and 7, respectively). As has been noted by other authors /35,46/ in this temperature region vacancies are mobile and form vacancy clusters while dislocation loops break up. Therefore recovery of ρ_o and T_c may be attributed to the annealing of these defects.

For rough substrates ρ_o-values of about 50 $\mu\Omega$cm are observed at low substrate temperatures. As argued above, the high values of ρ_o may be at-tributed to dislocations. This is supported by the work of Schultz /44/ who observed a rather high value of 6.7×10^{-17} Ωcm^3/dislocation, in Re. Using this value it can be estimated that 7×10^{11} dislocations/cm^2 are present in the films grown on rough substrates. The existence of 10^{12} dislocations/cm^2 in thin films is not unrealistic /36/, especially for rough substrates, where strains produced during film growth in the contact area of microcrystals with different orientations are immediately compensated by the formation of misfit dislocations. The influence of smaller defects can also not be excluded.

Inductive T_c-values for films grown on rough substrates are not only lower but also have larger transition widths, ΔT_c, than for polished films at low substrate temperatures. This can be explained by the assumption that vacancies are inhomogeneously distributed due to the presence of a large number of dislocations.

The decrease of ρ_0 as a function of substrate temperature for rough substrates starts around 900 K (0.26 T_m) and attains a saturation value of 7.3 $\mu\Omega$cm around 1330 K (0.39 T_m). Kopetskii et al. /9/ have observed the annealing of dislocation loops above 1000 K (0.29 T_m). Thus the question as to the origin of the seven $\mu\Omega$cm which still exists in rough substrates remains open.There are two arguments indicating that this ρ_0-value does not result from the Al_5Re_{24} phase. First, RBS-measurements show that the Al is not homogeneously distributed in the Re-film and thus Al_5Re_{24} has formed at the interface with little or no effect on ρ_0. Second, the intensity measurements of X-ray lines indicate that the Al_5Re_{24} phase component increased from 1 to 7% (as compared to Re) with increasing substrate temperature whereas ρ_0 decreased. Therefore, this phase cannot be responsible for the high values of ρ_0 which may, however, be attributed to partial dislocations and stacking faults still existing in these films.

A T_c-value of 3.35 K is reported for Al_5Re_{24} /34/. As this value is not observed in the present work it may be concluded that the Al_5Re_{24} formed is in a highly defective state with T_c-values below 1.7 K.

4.2 Electrical Size Effects and T_c:

As mentioned above, it was possible to prepare single-crystalline Re films with ρ_{RT}- and T_c-values of 18.0 $\mu\Omega$cm and 1.7 K, respectively. Since these values are comparable to the bulk ρ_{RT}- and T_c-values, it was possible to study the electrical size effect and thickness dependence of T_c.

The main goal of size effect measurements is to get information on the mean free path of electrons. At room temperature the product $l_0 \cdot (1-P)$ is usually determined, where P is specular scattering factor and may even be negative /50/. At low temperatures near LNT, the condition $l_0 \gg t$ is usually fulfilled and it is possible to determine separate values for l_0 and P as has been shown in section 3.1.2.2. Together with the known temperature dependence of the resistivity for Re single crystals /51/, a value of $(4.5 \pm 0.3) \cdot 10^{-11}$ Ωcm^2 for the product $\rho(T) \cdot l_0(T)$ has been determined at LNT. Generally, this product is considered to

be temperature independent. Thus knowing the value of the resistivity at RT /1/, l_o(RT) has been calculated to be 250 ± 24 Å. Substitution of l_o(RT) in the product l_o(1-P), results in a P-value of 0.05 ± 0.03 which for simplicity, was approximated by zero. From the analysis of the temperature co-efficient of resistivity data using P equal to zero a somewhat higher value i.e. 360 ± 65 Å was obtained for l_o(RT). The value of l_o at RT determined here is of the same order of magnitude as for other transition metals such as Pt /52/ and Ta /53/. Dimitriev et al. /54/ have determined a value of 14.3 x 10^{-11} Ωcm^2 for the product $\rho(T) \cdot l_o(T)$. This value is a factor 3.2 larger than those obtained here. The reason for this discrepancy may be that these films had very high resistivity values of the order of 150 to 200 $\mu\Omega cm$ at room temperature, possibly resulting from the presence of a metastable phase of Re.

For polycrystalline films (Fig.10), a value of 1370 Å was obtained for l_o(1-P). Assuming that P = 0 is also valid here, an unrealistically large value of 1370 Å for l_o(RT) is obtained. The polycrystalline films had more defects as compared to single-crystalline films which is indicated by their high T_c and resistivity values. From this fact a smaller value of l_o(RT) is to be expected. To meet this requirement a negative P-value, which is not allowed in Fuchs-Sondheimer theory, has to be chosen. Thus it may be concluded that the Fuchs-Sondheimer theory can only be applied successfully to single-crystalline films.

Reed et al. /55/ have measured a resistivity ratio, r of the order of 43000 for an Re single crystal which gives a resistivity value of 4.19 x 10^{-10} Ωcm at LHeT. Using this value of resistivity and the product $\rho(T) \cdot l_o(T)$, the calculated l_o(LHeT) value is 10^7 Å. In the literature /40/ a value of 33000 to 53000 Å for l_o(LHeT) using five Re single crystals has been calculated. The estimated value of 5494 ± 2000 Å, for l_o(LHeT), (see section 3.1.2.2) appears to be very small. This leads to the conclusion that for the estimation of l_o at LHeT, the thickness dependence of resistivity cannot be used because at these temperatures the resistivity is determined by the scattering of conduction electrons from defects. The resistivity ratio at RT and LNT for a highly pure Re single crystal is nine while this ratio for the films investigated here was seven. Thus the resistivity in this temperature region changes linearly and the value of l_o(LNT) calculated here is reliable.

Using current theories /56/ it is possible to calculate l_o(RT) from experimentally determined values of the Fermi velocity /57/, density of states, $N(E_F)$ /58/, cell volume and resistivity at RT. A value of 125 Å calculated for l_o(RT) is a factor of 2 smaller than the experimental value. This is in reasonable agrement keeping in mind that these theories /56/ are based on many assumptions.

It is interesting to note that the films in the thickness region of 300 to 400 $\overset{o}{A}$ showed enhanced T_c-values. This thickness correspond to the average grain size as given in Table 6. Thus the enhanced defect production by microcrystalline islands which just come in contact may cause the enhanced T_c-values here. At thicknesses below 300 $\overset{o}{A}$ the films are no longer superconducting at temperatures above 1.4 K. This maybe due to the fact that these films have high ρ_o-values which makes electron-phonon coupling through the grains impossible and leads to non-superconducting films.

4.3 Ion Induced Intrinsic Defects:

In ion irradiation experiments it was shown that due to the rather inhomogeneous defect distribution in films, resistive T_c measurements are more suitable because they register T_c-changes in a small volume fraction of the Re films. In contrast the inductive T_c seems to register changes as a volume effect and provide more information about the distribution of defects which are responsible for the T_c-enhancements. Thus in such experiments both resistive and inductive T_c-measurements are advised.

It was shown in section 2.2.1 that the energy loss due to nuclear collisions was 8 to 20 eV/$\overset{o}{A}$ for N-ion irradiation as compared to Ar-ion irradiation where it was 69 to 105 eV/$\overset{o}{A}$. Therefore it is reasonable to compare the changes in $\Delta\rho_o$ and T_c at a constant value of the deposited energy density, Q, instead of at constant fluence where different amounts of damage would be produced by N- and Ar-ions due to their different energy losses in nuclear collisions. For this comparison the damage profiles were calculated /19/ and estimates were made over the film thickness for the energy losses by nuclear collisions. These are then multiplied with the ion fluence to get the Q-values in eV/cm^3 which are plotted against $\Delta\rho_o$, resistive- and inductive-T_c for N- and Ar-irradiations in Fig. 30.

This Fig. shows that the increase in $\Delta\rho_o$ from N- and Ar-irradiation is the same as a function of Q-value up to 10^{25} eV/cm^3. Thus it can be concluded that the damage production and distribution is independent of the ion species up to Q-values of about 10^{25} eV/cm^3. Calculations in section 3.2.1.1 have shown that for the low fluence region below 10^{13} ions/cm^2 about 81% (N-ions) to 89% (Ar-ions) of the Frenkel pairs (Fig. 13) are annealed in stage I. This is in confirmation with the work of Heyden et al. /59/ and Coltmann et al. /60/. They observed

Fig. 30
Changes in $\Delta\rho_O$ resistive
and inductive T_c-values
as a function of deposited
energy density.
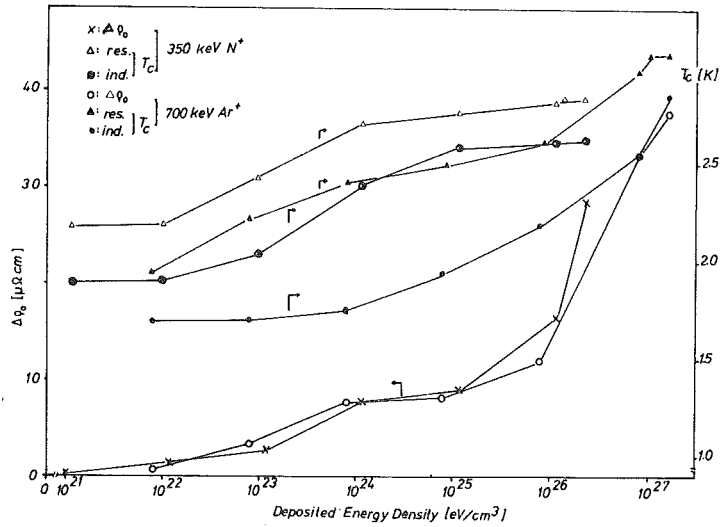
that about 75% of radiation-induced resistivity is recovered, up to 300 K.
The sharp increase of $\Delta\rho_O$ for Q-values above 10^{26} eV/cm^3 is probably a result
of dislocations. In section 3.2.1.1, the production rate of dislocations is
estimated to be 2×10^{-6} dislocations/ion.

The increase in resistive T_c-values shows the same functional dependence
on Q-value after N- and Ar-irradiations, however, the resistive T_c-values for
N-irradiations are consistently higher than those for Ar-irradiations. This
results from the fact that the pre-irradiated T_c-value was higher for the film
irradiated with N-ions. Thus radiation damage produced during irradiation adds
to the pre-irradiated damage of the film.

The inductive T_c-values, however, increased more sharply for N-irradiations
than for the Ar-irradiations (Fig. 30). As was discussed in section 3.2.2.1,
this could result from N-ions coming to rest at the interface between Re-film
and the substrate. This amount was between 0.05 and 0.2 at% depending on the
fluence value.

Isochronal annealing results for high and low dose N-ion irradiation
are summarized in Fig. 31. The ρ_O and T_c annealing spectra after irradiation
with 2×10^{17} N-ions/cm^2 indicate 4 recovery peaks: Stage II, at 0.15 T_m;
Stage IV at 0.23 T_m and Stage V at 0.28 T_m and 0.33 T_m. Similar results, which
are not plotted, were obtained for Ar-irradiaitons with the corresponding val-
ues: 0.15 T_m at Stage II; 0.23 T_m at Stage IV and 0.28 T_m and 0.33 T_m at
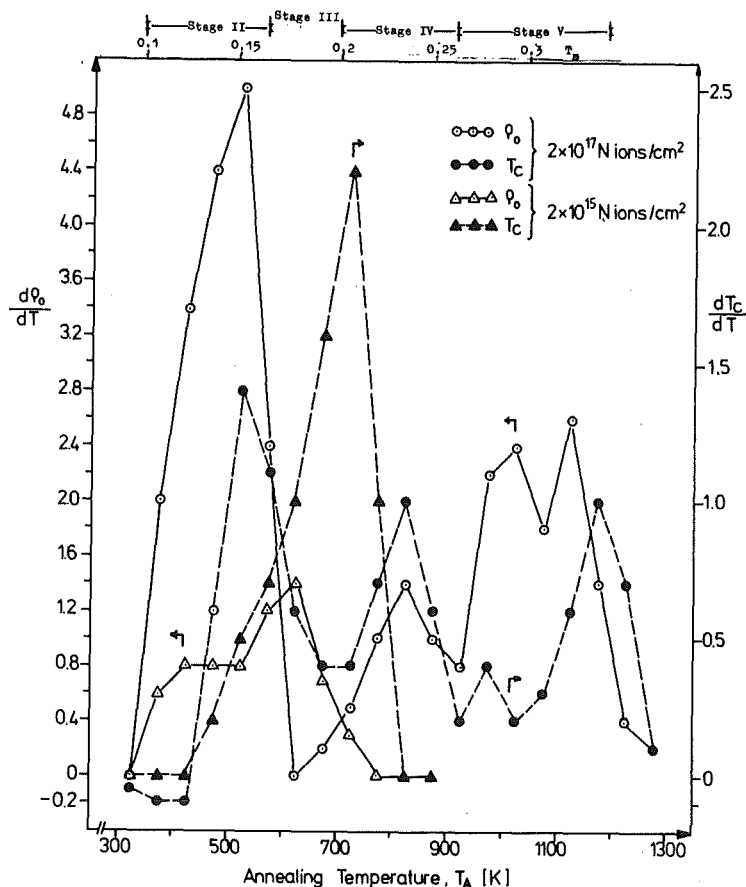Stage V.

Fig. 31
Isochronal annealing
spectra of Re-thin film
after irradiations at RT
with 4 x 10^{15} and
2 x 10^{17} N-ions/cm^2.
Solid line indicates re-
covery of inductive ρ_o.

The ρ_o- and T_c-annealing spectra after low dose nitrogen irradiation indicate
2 recovery peaks: Stage II at 0.14 T_m for both ρ_o and T_c (with of small contri-
bition); Stage III at 0.17 T_m, and 0.20 T_m for ρ_o and T_c, respectively.

To find out which kind of defects are mobile in the various stages,
the recovery of ρ_o for neutron irradiated samples /35/ is compared with these
results. Arguments are given in Ref. /35/ to identify the main annealing peak
observed at 0.19 T_m with Stage III. The other annealing stages can then be
attributed accordingly.

At Stage V the vacancy clusters dissociate and the vacancies annihilate
at the interstitial loops so that all damage should be removed. Stage V is most
pronounced for high dose Ar- and N-irradiated polycrystalline samples, however,
complete recovery was not observed. From energy dependent He-ion channeling mea-
surements /61/ on Re single crystals irradiated with 2 x 10^{17} Ar-ions/cm^2 and
annealed at 1275 K predicted the existence of stacking faults. Such partial dis-
locations or stacking faults might be responsible for the observed radiation in-
duced residual resistance which survived the annealing process after Stage V.

Stage IV which exists between 0.2 to 0.26 T_m is attributed to the annealing of small vacancy clusters which disappear in favour of larger ones. This Stage is small and not well pronounded in ion irradiated Re-films although continuous recovery is observed in this temperature region.

For Stage III, vacancies are thought to migrate and agglomerate or to annihilate at interstitial clusters. Stage III which was the main recovery peak for ρ_o in Ref. 35 is clearly observed for the low dose nitrogen irradiated sample. In the high dose irradiated samples this recovery stage might be burried in the huge recovery peak for Stage II observed for these samples. Stage III is clearly seen for the ρ_o-recovery of low dose irradiated samples. It is interesting to note that the T_c-recovery for such samples is shifted to somewhat higher temperatures and annealed completely at the end of Stage III. This may be a result of the presence of N-ions in the film which become mobile at the end of this Stage as is shown later.

Stage II is attributed to the growth of interstitial clusters and to glide and climb processes of loops under their mutual strain fields. Such processes are pronounced for high dose irradiated samples, but are of minor importance for low dose irradiated samples (Fig. 31).

The T_c-recovery of high dose irradiated samples is connected with all stages observed for ρ_o-recovery in roughly equal amounts. This is a clear indication that the vacancies are pinned to dislocations and the T_c-value does only depend on the dislocation density surviving each annealing stage. In contrast to the ρ_o-recovery, the T_c-recovery is completed at 1275 K. Thus dilatation zones of extended defects are also excluded as being responsible for T_c-enhancements. These results support the findings of previous workers /2,3/ who argued that vacancies are responsible for the enhanced T_c-values observed during plastic deformation of bulk Re. Dislocations can be excluded as defects which influence T_c directly, at least after low dose N-irradiation. For low dose N-irradiation the ρ_o increase was accompanied with T_c-enhancements and complete annealing was observed for ρ_o and T_c in Stage III. For high dose N- and Ar-irradiated samples the annealing behaviour of T_c can be explained by assuming that vacancies are pinned to extended defects and being successively released during the annelaing procedure.

4.4 Impurity Stabilized Defects and Metastable Phases:

As mentioned earlier, the purpose of homogeneous ion implantation was to produce intrinsic defects and impurity stabilized defects or metastable phases separately and to study their influence on the resistivity, T_c and structure of the Re-films. Table 12 presents the comparison for $\Delta\rho_o$- and T_c-values of ion irradiation and implantation experiments at a constant value of the deposited energy density of 1.5×10^{26} eV/cm^3.

Table 12

Comparison of increases in T_c, $\Delta\rho_o$ and cell volume, V_c at a constant value of the deposited energy density after implantation and irradiation of the N- and Ar-ions.

	T_c K	$\Delta\rho_o$ [$\mu\Omega$cm]	increase in cel vol. [$Å^3$]	mechanism
1 at% Ar	2.7	20.4	1.5%	impl.
1.9×10^{16} Ar-ions/cm^2	2.3	14.1	1.6%	irr.
5.2 at% N	2.8	31.7 ·	2.6%	impl.
1.3×10^{17} N-ions/cm^2	2.5	16.2	2.5%	irr.

It is seen that Ar implantation produces additional increase of 0.4 K and 6.3 $\mu\Omega$cm in T_c and $\Delta\rho_o$ then Ar-irradiation. Similarly N-ion implantation causes an increase of 0.3 K and 15.5 $\mu\Omega$cm in T_c and $\Delta\rho_o$, respectively, compared to N-irradiations. Thus it is concluded that a T_c-saturation level of about 3.0 K is reached due to the formation of impurity defects-complexes. Nitrogen-defect-complexes are rather effective electron scattering centers indicated by the relatively high values of $\Delta\rho_o$.

N-concentrations between 6 and 50 at% implanted at RT and LNT temperature formed at least two metastable phases. First phase was formed at 9 at% N ($ReN_{0.09}$). The structure of this phase (Table 11 column 1) could not be identified. This phase was also formed after implantation at LNT and 475 K. Maximum inductive and resistive T_c-values were 3.5 K and 4.0 K, respectively.

Above 12 at% N, second metastable phase was obtained which had a fcc(B1) structure. The lattice parameter of this phase was found to depend on the N-con- centration and varied from 3.93 to 4.02 Å as the concentration was changed from

13 to 50 at%. The T_c-value also increased with the increasing lattice parameter. It is supposed that this phase has an fcc lattice with NaCl structure and a lattice parameter of 4.02 Å. An increase in lattice parameter and T_c with N-concentrations is usually observed for nitrides with B1 structure.

It was interesting to note that at 9 and 45 at% N high stress values of the order of 14 x 10^{10} and 98 x 10^{10} dynes/cm^2, respectively were observed (Fig. 24). The pre-implantation stress value was 3 x 10^9 dynes/cm^2. At the same concentrations the new phases were observed (Table 11). Thus it is concluded that formation of these phases is accompanied by the appearence of high stresses which disappeared just after these phases are formed as it was shown in Fig. 26 for ReN$_{0.09}$. From the best available information such an effect has not been reported in literature.

Storage of ReN even at RT caused decomposition indicating that it is a metastable phase. Annealing experiments and structural studies have shown that both above mentioned phases decomposed completely above 645 K. Hahn and Konrad /31/ have reported ReN$_{0.43}$ (a = 3.93 Å) and a decomposition temperature between 553 and 625 K.

For N-implantation at concentrations above 42 at% LNT all X-ray lines disappeared. Inductive and resistive T_c-values of 5 and 6 K, respectively, with ρ_{RT}-value of 320 $\mu\Omega$cm were obtained. Both this amorphous phase and ReN decomposed at 645 K. It was not possible to decide if this phase was a micro-crystalline ReN or amorphous Re. Matthias and Zachriasen /62/ have reported a ReN$_{0.34}$ with crystallite size of 20 to 26 Å and a T_c-value of 4 K. Because of the relatively high T_c values observed here, it was assumed that an amorphous phase of Re was stabilized. In order to prove this assumption P-ions were implanted at LNT because rhenium phosphides are known to be non-superconductors.

At 20 at% P, an amorphous phase was obtained with a T_c-value of 7K measured both resistively and inductively. No x-ray lines from Re-phosphides could be detected. Using the assumption that like crystalline phosphides microcrystalline Re-phosphides are also not superconducting, this phase was identified as amorphous Re. This phase decomposed above 925 K. Thus an amorphous phase of rhenium stabilized by phosphorous has been obtained with a T_c-value of 7 K.

References:

/1/ P.E. Frieberthauser, H.A. Notarys: J.Vac. Sc. Techl. 7 (1970) 485

/2/ J.K. Hulm, B.B. Goodman: Phys. Rev. 106 (1957) 659

/3/ W. Buckel: Supraleitung; Grundlagen und Anwendungen, Physik Verlag (1977)

/4/ A.R. Miedema: J. Phys. F, Metal Phys. 4 (1974) 120

/5/ C.W. Chu, W.L. McMillan, H.L. Luo: Phys. Rev. B3 (1971) 3757

/6/ C.W. Chu, T.F. Smith, W.E. Gardner: Phys. Rev. Lett. 20 (1968) 198

/7/ O. Meyer: J. Jap. Soc. Appl. Phys. 44 (1975) 23

/8/ J.J. Hauser, E. Buehler: Phys. Rev. 125 (1962) 142

/9/ T.V. Kopetskii, M.M. Myshlyaev, N.I. Novochatskai, N.A. Tulina, V.A. Yukhanov: Phys. Stat. Sol. 16 (1973) 307

/10/ L.F. Mattheiss: Phys. Rev. 151 (1966) 450

/11/ F. Heiniger, E. Bucher, J. Müller: Phys. Kond. Materie 5 (1966) 243

/12/ T.H. Geballe: Rev. Mod. Phys. 36 (1964) 134

/13/ V.M. Polovov, N.A. Tulina, N.M. Gavrilov: Sov. J. Low Temp. Phys. 3 (1977) 604

/14/ G. Carter, J.S. Colligon: Ion Bombardment of Solids, Heinemann Educ. Books Ltd., London (1968)

/15/ P. Sigmund: Rev. Roum. Phys. 17 (1972) 823

/16/ G. Dearnaley, J.H. Freemann, R.S. Nelson, J. Stephan: Ion Implantation, North Holland Publ. Co., Amsterdam (1973)

/17/ K.G. Langguth: Dissertation, University of Karlsruhe, KfK 2476 (1977)

/18/ P. Ziemann: Dissertation, University of Karlsruhe, KfK 2562 (1977)

/19/ J.P. Biersack, L.G. Haggmark: Nuc. Instr. Methods 174 (1980) 257

/20/ M.W. Thompson: Defects and Radiation Damage in Metals, Cambridge University, Press, (1969)

/21/ H. Vandenborre, L. Stals, J. Cornelis, J. Nihoul: Rad. Effects 21 (1974) 137

/22/ G. Linker: KfK 2357 (1976) 86

/23/ J. Linhard, M. Scharff, H.E.Schiøtt: Matt. Fys. Medd. 33 (1963) No. 14

/24/ W.K. Chu, J.W.Mayer, M.A. Nicolet: Backscattering Spectrometry, Academic Press (1978) ch. 3

/25/ J.W. Mayer, E. Rimini: Ion beam handbook for material analysis, Academic Press (1977)

/26/ U. Schneider, J. Geerk: KfK 3051 (1980) 142

/27/ W. Schneider: KfK Externer Bericht 6/69-4 (1969)

/28/ R. Feder, B.S. Berry: J. Appl. Cryst. 3 (1970) 372

/29/ H. Neff: Grundlagen und Anwendung der Röntgen Feinstruktur Analyse,
R. Oldenburg, München (1962)

/30/ C.W. Chu, T.F. Smith, W.E. Gardner: Phys. Rev. B1 (1970) 214

/31/ von H. Hahn, A. Konrad: Z. Anorg. Allg. Chem. 264 (1951) 174

/32/ M.L. Gimpl, N. Fushillo, A.D. McMas: Trans. AIME 236 (1966) 331

/33/ E.M. Savitskii, M.A. Tylkina: Study and Use of Rhenium Alloys, Amerind
Publishing Co. New Dehli (1978)

/34/ E. Bucher, F. Heiniger, J. Müller: Phys. Kond. Materie 2 (1964) 210

/35/ H. Vandenborre, L. Stals, J. Nihoul: Phys. Stat. Sol. 35 (1969) 1009

/36/ K.L. Chopra: Thin Film Phenomena, McGraw Hill, N.Y. (1969)

/37/ K. Fuchs: Proc. Camb. Soc. 34 (1938) 100

/38/ E.H. Sondheimer: Adv. Phys. 1 (1952) 1

/39/ G. Fischer, H. Hoffmann, J. Vancea: Phys. Rev. 22B (1980) 6065

/40/ R. Schreiber: Ph. D Thesis, Rice University (1974)

/41/ K.L. Merkle, L.R. Singer: Appl. Phys. Lett. 11 (1967) 35

/42/ G.H. Kinchin, R.S. Pease: Rep. Prog. Phys. 18 (1955) 1

/43/ P. Lucassen: in Fundamental Aspects of Radiation Damage in Metals
Conf. 751006-P1, U.S. ERDA, Oak Ridge, Tenn. (1975)

/44/ Schultz in D. Dew-Hughes, M.J. Witcomb: Phil. Mag. 26 (1972) 73

/45/ S.T. Picraux, E. Rimini, G. Foti, S.U. Campisano: Phys. Rev. B18
(1978) 2078

/46/ J.L. Brimhall, B. Mastel: Phil. Mag. 12 (1965) 419

/47/ von H. Haraldsen: Z. Anorg. Allgem. Chemie 221 (1935) 397

/48/ B.W. Roberts: J. Phys. Chem. Ref. Data 5 (1976) 581

/49/ V.A. Komashko, Yu V. Titenko, T.V. Belousov, I.D. Vojtovich: Ukr. Fiz.
Zh. v. 23 (1978) 155

/50/ D. Dayal, P. Wissmann: Thin Solid Films 44 (1977) 185

/51/ G.K. White, S.B. Woods: Phil. Trans. Roy. Soc. (London) A251 (1959) 273

/52/ G. Fischer: Dissertation, University of Regensburg (1979)

/53/ R.B. Marcus: J. Appl. Phys. 37 (1960) 3121

/54/ V.P. Dmitriev, A.K. Milai, A.F. Orlov: Sov. J. Low Temp. Phys. 1 (1975) 438

/55/ W.A. Reed, E. Fawcett, R.R. Soden: Phys. Rev. A139 (1965) 1557

/56/ L.F. Mattheiss, L.R. Testardi: Phys. Rev. 20B (1979) 2196

/57/ N.A. Tulina: Fiz. Met. Metalloved (USSR) 50 (1980) 747

/58/ F.J. Morin, J.P. Maita: Phys. Rev. 129 (1963) 115

/59/ R.R. Coltmann, C.E. Klabunde, J.K. Redman: Phys. Rev. 156 (1967) 715

/60/ G. von Heyden, H. Vandenborre, L. Stals, J. Nihoul: Rad. Effects 9
      (1971) 279

/61/ E. Friedland, A. ul Haq, M. Kraatz: KfK 3051 (1980) 114

/62/ B.T. Matthias, W.H. Zachariasen: J. Phys. Chem. of Solids 7 (1958) 98